

# **First Search for Heavy Neutral Leptons with IceCube DeepCore**

**Dissertation**  
zur Erlangung des akademischen Grades  
doctor rerum naturalium  
(Dr. rer. nat.)

im Fach: Physik  
Spezialisierung: Experimentalphysik

eingereicht an der  
Mathematisch-Naturwissenschaftlichen Fakultät  
der Humboldt-Universität zu Berlin

von  
**Leander Fischer M. Sc.**  
geboren am 24. Oktober 1992  
in Heidelberg

Präsidentin der Humboldt-Universität zu Berlin  
Prof. Dr. Julia von Blumenthal

Dekanin der Mathematisch-Naturwissenschaftlichen Fakultät  
Prof. Dr. Caren Tischendorf

### **Copyright Notice**

This book is released into the public domain using the CC-BY-4.0 code.

To view a copy of the CC-BY-4.0 code, visit:

<https://creativecommons.org/licenses/by/4.0/>

### **Colophon**

This document was typeset with the help of KOMA-Script and L<sup>A</sup>T<sub>E</sub>X using the open-source kaobook template class.

The source code of this thesis is available at:

[https://github.com/LeanderFischer/phd\\_thesis](https://github.com/LeanderFischer/phd_thesis)

## **Zusammenfassung**

Zusammenfassung ...

## **Abstract**

Abstract ...



# Todo list

adjust final vertical position of this reference . . . . .	1
Also cite this? Didn't find a good reference, only the press releases. . . . .	1
Introduce SM EW NC/CC Lagrangian to build upon in the next chapter . . . . .	3
Plot is missing + for W and 0 for Z boson. . . . .	3
Cite and/or sidenote this. . . . .	4
cite this . . . . .	4
cite neutrino oscillations/flavor conversions . . . . .	4
namedrop RH=sterile=HNL and why they are called like this based on the SM EW Lagrangian introduced above . . . . .	4
write some interlude to motivate atm. neutrinos as source for HNL searches/production etc. . . . .	8
Say something about atmospheric neutrino flux uncertainties, based on recent JP/Anatoli papers. . . . .	9
add current BF values from nufit or so? . . . . .	11
say something about how this changes with matter . . . . .	12
Re-write/re-formulate this section (copied from HNL technote). . . . .	12
Produce similar styled plot for these limits . . . . .	12
This section really needs to be re-written to motivate the search for HNLs from a more generic point of view (e.g. to explain neutrino masses) . . . . .	13
This section definitely needs to be elaborated in a little more detail . . . . .	13
Not adding information about the case where the neutrinos have Dirac or pseudo-Dirac masses . . . . .	13
maybe I want a figure for this, or not so important? (YELLOW) . . . . .	17
Elaborate whether this is the case (show it in a plot?). Discuss directionality of cascades in general. (ORANGE) . . . . .	17
fix caption of this figure (RED) . . . . .	18
fix caption of this figure (RED) . . . . .	19
one half sentence on why this number was chosen? (ORANGE) . . . . .	20
make one figure, where the two selected regions are highlighted? (RED) . . . . .	22
fix caption (RED) . . . . .	22
re-make normalized? (ORANGE) . . . . .	23
fix caption (RED) . . . . .	23
re-make normalized? (ORANGE) . . . . .	23
fix caption (RED) . . . . .	23
circle back to the energy distributions I showed somewhere else, and state how the cascade energies are distributed in general (ORANGE) . . . . .	24
fix caption of this figure (RED) . . . . .	25

describe the "good fit" selection when I first show plots that use it (ORANGE) . . . . .	25
add some 1D resolution plots (ORANGE) . . . . .	25
fix caption of this figure (RED) . . . . .	26
fix caption of this figure (RED) . . . . .	26
fix caption of this figure (RED) . . . . .	27
fix caption of this figure (RED) . . . . .	27
fix caption of this figure (RED) . . . . .	27
Make plot to show efficiency of the OscNext selection for HNL events. (ORANGE) . . . . .	27
Plot energy (true total) and true decay length across the different levels (ORANGE) . . . . .	27
Make table with the rates across the different levels for benchmark mass/mixing (ORANGE) . . . . .	27

# Contents

<b>Abstract</b>	<b>iii</b>
<b>Contents</b>	<b>vii</b>
<b>1 Standard Model Neutrinos and Beyond</b>	<b>1</b>
1.1 The Standard Model . . . . .	1
1.1.1 Fundamental Fields . . . . .	1
1.1.2 Electroweak Symmetry Breaking . . . . .	2
1.1.3 Fermion Masses . . . . .	3
1.1.4 Weak Interactions after Symmetry-Breaking . . . . .	3
1.2 Beyond the Standard Model . . . . .	3
1.2.1 Mass Mechanisms . . . . .	4
1.2.2 Neutrino Minimal Standard Model ( $\nu$ MSM) . . . . .	5
1.2.3 Observational Avenues for Right-Handed Neutrinos . . . . .	5
1.2.4 Searching for Heavy Neutral Leptons . . . . .	6
1.3 Atmospheric Neutrinos as Source of Heavy Neutral Leptons . . . . .	8
1.3.1 Production of Neutrinos in the Atmosphere . . . . .	8
1.3.2 Interactions with Nuclei . . . . .	9
1.3.3 Oscillations . . . . .	11
1.3.4 Testing Heavy Neutral Leptons with Atmospheric Neutrinos . . . . .	12
<b>2 Detecting Low Energetic Double Cascades</b>	<b>17</b>
2.1 Reconstruction . . . . .	17
2.1.1 Table-Based Minimum Likelihood Algorithms . . . . .	17
2.1.2 Optimization for Low Energy Events . . . . .	18
2.1.3 Performance . . . . .	20
2.2 Double Cascade Classification . . . . .	24
2.3 Generic Double Cascade Performance . . . . .	24
2.3.1 Idealistic Performance . . . . .	25
2.3.2 Realistic Performance . . . . .	25
2.3.3 Low Energy Event Selection Efficiency . . . . .	27
<b>Bibliography</b>	<b>31</b>



# List of Figures

1.1	Feynman diagrams of neutrino weak interactions . . . . .	3
1.2	HNL decay widths . . . . .	8
1.3	Atmospheric neutrino fluxes . . . . .	9
1.4	Neutrino-nucleon deep inelastic scattering . . . . .	10
1.5	Total inclusive neutrino-nucleon cross-sections . . . . .	10
1.6	Current $ U_{\tau 4}^2  - m_4$ limits . . . . .	12
1.7	Feynman diagram of HNL up-scattering process . . . . .	14
1.8	Feynman diagram of HNL decay . . . . .	14
1.9	HNL branching ratios . . . . .	15
2.2	short . . . . .	19
2.3	Preliminary 2-d reconstructed versus true cascade energy resolutions . . . . .	21
2.4	Preliminary 2-d reconstructed versus true decay length resolutions . . . . .	22



# List of Tables

1.1 Standard model fermions . . . . .	2
---------------------------------------	---



# Standard Model Neutrinos and Beyond

1

## 1.1 The Standard Model

The *Standard Model (SM)* of particle physics is a Yang-Mills theory [1] providing very accurate predictions of weak, strong, and *electromagnetic (EM)* interactions. It is a relativistic quantum field theory that relies on gauge invariance, where all matter is made up of fermions, which are divided into quarks and leptons, and bosons describe the interactions between the fermions that have to fulfil the overall symmetry of the theory. Leptons are excitations of Dirac-type fermion fields.

The initial idea of the theory is associated with the works of Weinberg [2], Glashow [3], and Salam [4], that proposed a unified description of EM and weak interactions as a theory of a spontaneously broken  $SU(2) \times U(1)$  symmetry for leptons, predicting a neutral massive vector boson  $Z^0$ , a massive charged vector boson  $W^\pm$ , and a massless photon  $\gamma$  as the gauge bosons. The Higgs mechanism [5], describing the breaking of the symmetry, predicts the existence of an additional scalar particle, the Higgs boson, giving the  $W^\pm$  and  $Z^0$  bosons their mass. The Higgs boson was discovered in 2012 at the LHC.

Gell-Mann and Zweig proposed the quark model in 1964 [6, 7], which was completed by the discovery of non-abelian gauge theories [8] to form the  $SU(3)$  symmetry of the strong interaction called *quantum chromodynamics (QCD)*. QDC describes the interaction between quarks and gluons which completed the full picture of the SM in the mid-1970s. Together with the electroweak theory, the SM is a  $SU(3)_C \times SU(2)_L \times U(1)_Y$  local gauge symmetry, with the conserved quantities  $C$ , *color*,  $L$ , *left-handed chirality*, and  $Y$ , *weak hypercharge*.

In the following, the basic properties of the SM are described, following the derivations of [9, 10].

### 1.1.1 Fundamental Fields

Fermions in the SM are Weyl fields with either *left-handed (LH)* or *right-handed (RH)* chirality, meaning they are eigenvectors of the chirality operator  $\gamma_5$  with  $\gamma_5 \psi_{R/L} = \pm \psi_{R/L}$ . Only LH particles transform under  $SU(2)_L$ . The Higgs field is a complex scalar field, a doublet of  $SU(2)_L$ , which is responsible for the spontaneous symmetry breaking of  $SU(2)_L \times U(1)_Y$  to  $U(1)_{\text{EM}}$ . Local gauge transformations of the fields are given by

$$\psi \rightarrow e^{ig\theta^a(x)T^a} \psi , \quad (1.1)$$

where  $g$  is the coupling constant,  $\theta^a(x)$  are the parameters of the transformation, and  $T^a$  are the generators of the group, with  $a$  counting them. The number of bosons is dependent on the generators of the symmetry groups, while the strength is defined by the coupling constants. There are eight massless gluons corresponding to the generators of the  $SU(3)_C$  group. These

1.1 The Standard Model	1
1.2 Beyond the Standard Model . . . . .	3
1.3 Atmospheric Neutrinos as source of Heavy Neutral Leptons . . . . .	8

[1]: Yang et al. (1954), "Conservation of Isotopic Spin and Isotopic Gauge Invariance"

[2]: Weinberg (1967), "A Model of Leptons"

[3]: Glashow (1961), "Partial-symmetries of weak interactions"

[5]: Higgs (1964), "Broken symmetries, massless particles and gauge fields"

Also cite this? Didn't find a good reference, only the press releases.

[6]: Gell-Mann (1964), "A Schematic Model of Baryons and Mesons"

[7]: Zweig (1964), "An  $SU(3)$  model for strong interaction symmetry and its breaking. Version 2"

[9]: Giunti et al. (2007), *Fundamentals of Neutrino Physics and Astrophysics*

[10]: Schwartz (2013), *Quantum Field Theory and the Standard Model*

mediate the strong force which conserves color charge. The  $W_1, W_2, W_3$ , and  $B$  boson fields of the  $SU(2)_L \times U(1)_Y$  group are mixed into the massive bosons through spontaneous symmetry breaking as

$$W^\pm = \frac{1}{\sqrt{2}}(W_1 \mp iW_2) \quad (1.2)$$

and

$$Z^0 = \cos \theta_W W_3 - \sin \theta_W B, \quad (1.3)$$

with  $\theta_W$  being the *Weinberg angle*. The massless photon field is given by

$$A = \sin \theta_W W_3 + \cos \theta_W B \quad (1.4)$$

and its conserved quantity is the EM charge  $Q$ , which depends on the weak hypercharge,  $Y$ , and the third component of the weak isospin,  $T_3$ , as  $Q = T_3 + Y/2$ .

	Type			$Q$
quarks	u	c	t	+2/3
	d	s	b	-1/3
leptons	$\nu_e$	$\nu_\mu$	$\nu_\tau$	0
	e	$\mu$	$\tau$	-1

**Table 1.1:** Fermions in the Standard Model. Shown are all three generations of quarks and leptons with their electric charge  $Q$ .

Fermions are divided into six quarks and six leptons. Weak, strong, and EM force act on the quarks, and they are always found in bound form as baryons or mesons. Leptons do not participate in the strong interaction and only the electrically charged leptons are massive and are effected by the EM force, while neutrinos are massless and only interact via the weak force. Each charged lepton has an associated neutrino, which it interacts with in *charged-current (CC)* weak interactions, that will be explained in more detail in Section 1.1.4. The fermions are listed in Table 1.1.

### 1.1.2 Electroweak Symmetry Breaking

To elaborate the process of spontaneous symmetry breaking through which the gauge bosons of the weak interaction acquire their masses, the Lagrangian of the Higgs field is considered as

$$\mathcal{L}_{\text{Higgs}} = (D_\mu \Phi^\dagger)(D^\mu \Phi) - \lambda \left( \Phi^\dagger \Phi - \frac{v^2}{2} \right)^2, \quad (1.5)$$

with parameters  $\lambda$  and  $v$ , where  $\lambda$  is assumed to be positive.  $\Phi$  is the Higgs doublet, which is defined as

$$\Phi = \begin{pmatrix} \Phi^+ \\ \Phi^0 \end{pmatrix}, \quad (1.6)$$

with the charged component  $\Phi^+$  and the neutral component  $\Phi^0$ . The covariant derivative is given by

$$D_\mu = \partial_\mu - ig_2 \frac{\sigma^i}{2} W_\mu^i - \frac{1}{2}ig_1 B_\mu, \quad (1.7)$$

with the Pauli matrices  $\sigma^i$  and the gauge boson fields  $W_\mu^i$  and  $B_\mu$  of the  $SU(2)_L$  and  $U(1)_Y$  groups, respectively. The coupling constants  $g_2$  and  $g_1$  are the respective coupling constants which are related to the Weinberg angle as  $\tan \theta_W = \frac{g_1}{g_2}$ . The Higgs potential has a non-zero *vacuum expectation value (vev)* at the minimum of the potential at  $\Phi^\dagger \Phi = \frac{v^2}{2}$ . Since the vacuum is electrically neutral, it can only come from a neutral component of the Higgs

doublet as

$$\Phi_{\text{vev}} = \frac{1}{\sqrt{2}} \begin{pmatrix} 0 \\ v \end{pmatrix}. \quad (1.8)$$

### 1.1.3 Fermion Masses

The mass term for charged fermions with spin-1/2 is given by

$$\mathcal{L}_{\text{Dirac}} = m(\bar{\Psi}_R \Psi_L - \bar{\Psi}_L \Psi_R), \quad (1.9)$$

composed of the product of left- and RH Weyl spinors  $\Psi_{L/R}$ . This term is not invariant under  $SU(2)_L \times U(1)_Y$  gauge transformations, but adding a Yukawa term

$$\mathcal{L}_{\text{Yukawa}} = -y \bar{L}_L \Phi e_R + h.c., \quad (1.10)$$

coupling the fermion fields to the Higgs field, recovers the invariance and gives the fermions their masses. Here,  $y$  is the Yukawa coupling constant and  $\bar{L}_L$  is the  $SU(2)_L$  doublet. With the vev, this results in the mass term for the charged leptons and down-type quarks of  $-m_e(\bar{e}_L e_R + \bar{e}_R e_L)$  with  $m_e = \frac{yv}{\sqrt{2}}$ . With  $\tilde{\Phi} = i\sigma_2 \Phi^*$ , a similar Yukawa term can be written as  $-y \bar{L}_L \tilde{\Phi} u_R + h.c.$ , which leads to the masses of the up-type quarks.

### 1.1.4 Weak Interactions after Symmetry-Breaking

#### Stuff from my MSc thesis to re-write:

In the SM, weak interactions are mediated by the three massive bosons  $W^+$ ,  $W^-$ , and  $Z^0$  [12]. The large boson masses ( $m_W \sim 80 \text{ GeV}$ ,  $m_Z \sim 90 \text{ GeV}$ ) result in a short range of the force of about  $10 \times 10^{-18} \text{ m}$ . Weak interactions carried by  $W^\pm$  bosons are called CC interactions, because charge is transferred between the interacting particles. In CC interactions, a neutrino is converted into its corresponding charged lepton or vice versa. Neutral current (NC) interactions are those mediated by  $Z^0$  bosons. Here no charge is transferred. The Feynman diagrams for CC and NC interactions are shown in Figure 1.1.

The observed phenomenon of neutrino oscillations (see Section 1.3.3) is based on the fact that there is a mass difference between the three neutrino mass eigenstates.

Introduce SM EW NC/CC Lagrangian to build upon in the next chapter

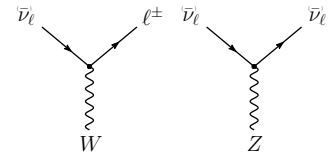


**Figure 1.1:** Feynman diagrams of charged-current (left) and neutral-current (right) neutrino weak interactions, taken from [11].

Plot is missing + for W and 0 for Z boson.

[12]: Thomson (2013), *Modern particle physics*

## 1.2 Beyond the Standard Model

#### Open questions related to neutrinos:

- ▶ question of neutrino nature, e.g. dirac or majorana?
- ▶ absolute mass values? (mass ordering + absolute mass scale)
- ▶ is there leptonic cp violation and what is the precise delta\_cp value?
- ▶ what are the mixing angle values and is there a flavor principle
- ▶ is there additional effects like steriles, non-standard, lorentz violation

Are the fundamentals of the SM described above enough to explain *all* observed phenomena? Gravity cannot be explained by the SM, as it is incompatible with general relativity. Neither can the SM explain some cosmological observations like dark matter, and the matter-antimatter asymmetry, and it does not predict neutrinos to have mass, which is experimentally proven by neutrino oscillations, so some extensions to the SM is needed in order to explain them.

Cite and/or sidenote this.

Standard cosmology ( $\Lambda$ CDM) assumes that equal amounts of matter and anti-matter were produced in the early universe. However, the universe today is dominantly made up of matter. This so-called *baryon asymmetry* can be measured by the difference between the number densities of baryons and anti-baryons normalized to the number density of photons as

$$\eta_B = \frac{n_B - n_{\bar{B}}}{n_\gamma} , \quad (1.11)$$

cite this

where  $n_B$ ,  $n_{\bar{B}}$ , and  $n_\gamma$  are the number densities of baryons, anti-baryons, and photons, respectively. Baryons are the dominant component with  $\eta_B$  being observed to be around  $6 \times 10^{-10}$ . Leptogenesis and EW baryogenesis are scenarios that could explain this phenomenon, where the former could be realized by the existence of heavy RH neutrinos.

- [13]: Davis et al. (1968), "Search for Neutrinos from the Sun"
- [14]: Fukuda et al. (1998), "Evidence for Oscillation of Atmospheric Neutrinos"
- [15]: Ahmad et al. (2002), "Direct Evidence for Neutrino Flavor Transformation from Neutral-Current Interactions in the Sudbury Neutrino Observatory"

cite neutrino oscillations/flavor conversions

The observation of neutrino flavor conversions and neutrino oscillations in a multitude of experiments[13–15] is the strongest evidence for physics beyond the SM measured in laboratories. The observation that neutrinos change their flavor while they propagate through space can only be explained, if at least two neutrinos have a non-zero mass. From the measurements and cosmological observations, we know that the masses are very small as compared to the lepton masses. Neither their existence, nor their smallness is not predicted by the SM, but adding additional RH neutrinos states to the theory could explain the origin of the observed non-zero neutrino masses and could be tested for by searching for corresponding signatures in experiments. But the addition of RH neutrino fields is not the only possible explanation for neutrino masses. Radiative neutrino mass mechanisms could also explain their origin and their smallness, but those would need the introduction of additional symmetries to the theory.

- [16]: Tanabashi et al. (2018), "Review of Particle Physics"
- [17]: Aker et al. (2022), "Direct neutrino-mass measurement with sub-electronvolt sensitivity"
- [18]: Alam et al. (2021), "Completed SDSS-IV extended Baryon Oscillation Spectroscopic Survey: Cosmological implications from two decades of spectroscopic surveys at the Apache Point Observatory"
- [19]: Aghanim et al. (2020), "Planck2018 results: VI. Cosmological parameters"

namedrop  
RH=sterile=HNL and  
why they are called like  
this based on the SM EW  
Lagrangian introduced  
above

Maybe also add this somehow: "From neutrino oscillation measurements the absolute mass scale cannot be determined, since they only depend on the mass differences, but there are upper limits on the sum of all neutrino masses from cosmological observations. These upper limits are typically between 0.3 and 1.3 eV [16]." "Actually 0.8 eV [17] from KATRIN and 1.2 eV [18, 19] from cosmological observations."

### 1.2.1 Mass Mechanisms

There are no RH neutrinos in the SM and therefore the mass mechanism described in Section 1.1.3, which couples the Higgs field to LH and RH Weyl fields, predicts them to be massless. From experimental observations it is known that at least two of the three neutrino generations need to have a non-zero mass. Assuming the existence of RH neutrinos fields  $\nu_R$ , one way of producing the neutrino masses is by adding a Yukawa coupling term

similar to the one for up-type quarks mentioned in Section 1.1.3, to write the full Yukawa Lagrangian as

$$\mathcal{L}_{\text{Yukawa}} = -Y_{ij}^e \bar{L}_L^i \Phi e_R^j - Y_{ij}^\nu \bar{L}_L^i \tilde{\Phi} \nu_R^j + h.c. , \quad (1.12)$$

with  $i, j$  running over the three generations of leptons  $e, \mu$ , and  $\tau$ , and  $Y^e$  and  $Y^\nu$  being the Yukawa coupling matrices. Diagonalizing the Yukawa coupling matrices through unitary transformations  $U^e$  and  $U^\nu$  leads to the **Dirac mass term** in the mass basis as

$$\mathcal{L}_{\text{Dirac}}^{\text{mass}} = \frac{v}{\sqrt{2}} (\bar{e}_L M_e e_R - \bar{\nu}_L M_\nu \nu_R) , \quad (1.13)$$

where  $M_e$  and  $M_\nu$  are the diagonal mass matrices of leptons and neutrinos, respectively. A purely Dirac mass term would not explain the smallness of the neutrino masses in a straightforward way. Only fine-tuning the Yukawa coupling constants to small values would lead to small neutrino masses.

An additional way of generating neutrino masses is by adding a Majorana mass term of the form

$$\mathcal{L}_{\text{Majorana}} = -\frac{1}{2} M_{ij} (\nu_R^i)^c \nu_R^j + h.c. , \quad (1.14)$$

with  $M_{ij}$  being the Majorana mass matrix and the indices  $i, j$  running over all  $N_R$  RH neutrino generations. The superscript  $c$  denotes the charge conjugate field. Combining the charge conjugated RH neutrino fields with the LH neutrino fields as

$$N = \begin{pmatrix} \nu_L \\ \nu_R^c \end{pmatrix} , \quad (1.15)$$

with  $\nu_R$  containing the  $N_R$  RH fields. The full neutrino mass Lagrangian is then given by the combined **Dirac and Majorana mass term** as

$$\mathcal{L}_{\text{Dirac+Majorana}}^{\text{mass},\nu} = \frac{1}{2} N^T \hat{C} M^{D+M} N + h.c. , \quad (1.16)$$

and the mass matrix is given by

$$M^{D+M} = \begin{pmatrix} 0 & (M^D)^T \\ M^D & M^R \end{pmatrix} . \quad (1.17)$$

On top of explaining the origin of neutrino masses itself, a combined Dirac and Majorana mass term could also solve the question of their smallness. If the mass of the RH neutrinos is very large, the masses of the active neutrino flavors is suppressed, which is known as *see-saw mechanism*.

## 1.2.2 Neutrino Minimal Standard Model ( $\nu$ MSM)

### 1.2.3 Observational Avenues for Right-Handed Neutrinos

- ▶ oscillations searches for light steriles
- ▶ potential searches for heavy steriles

### 1.2.4 Searching for Heavy Neutral Leptons

#### Colliders

**Current Measurements** LHC: proton-proton collider  $\text{sqrt}(s)$ : 7, 8, 13

ATLAS/CMS: nearly hermetic detectors around interaction, multiple searches for HNL scenarios LHCb: forward detector, designed to search for new particles in decays of heavy hadrons

Type I Seesaw Results:

HNL production in GeV range from : decays of heavy mesons, tau leptons, W bosons, H bosons, or top quarks HNL decays: to lepton number conserving (dirac), or lepton number conserving and violating channels (majorana), depending on mass and mixing parameters, prompt and displaced decays are possible

Atlas results set constraints on mixing with e and mu:

Atlas in minimal extension:  $10^{-6}$  with  $U_m u 4$  at 4-10 GeV same for CMS:  $10^{-5}$  with  $U_m u 4$  and  $U_e 4$  at 10-600 GeV

CMS: final state of 3 leptons (two opposite charged and nu) giving  $U_m u 4$   $4 * 10^{-7}$  at 8-14 GeV

the above mentioned (strong) constraints are mostly based on a model with one HNL coupling to one flavor in type 1 seesaw at least 2 are needed to see the two SM nu masses, both coupling to several flavors it was shown (cite) that re-interpreting these results with more than one HNL can lead to much weaker constraints and to compare results, the assumed model and couplings have to be considered the strong reduction in constraints is due to the opening of new channels, to which the search may not be sensitive

more complex scenarios are possible and might produce various signatures, but are harder to measure: extended gauge symmetries, effective field theories

type III seesaw (HNL as SM EW triplets) can be observed as they are produced in pairs (no active-sterile mixing needed) and result in multi lepton states and high pt jets  $\rightarrow$  strong exclusion of masses below 790 GeV

LHCb: low mass and high mass results (above below mW), competitive in low mass

low mass channel:  $B^+ \rightarrow \mu^+ N \rightarrow \pi^+ \mu^-$ , at order  $10^{-3}$  for  $U_m u 4$  at 0.5-3.5 GeV

high mass channel:  $W^+ \rightarrow \mu^+ \mu^+ \text{-jet}$ , at order  $10^{-3-10^{-2}} / 10^{-4-10^{-3}}$  for  $U_m u 4$  at 5-50 GeV for LNC/LNV

**Future Colliders** there is a shit ton of future colliders and/or experiments at the LHC planned, that have sensitivities to HNLs.. think about which/how to discuss them

## Nuclear Decay

novel approach to search for HNLs through energy-momentum conservation measurements in nuclear reactions

mixing of HNL with electron nu/nubar would cause irregularities, interpretable as limits in  $|U_{e4}|^2$  and m4

**Beta Decay** detect kinks in the energy spectra at  $Q - m_4 c^2$

m4 probable between energy detection threshold and Q value of the decay

tritium 3H: Q=18.6 keV

planned analysis in KATRIN and TRISTAN (1 to 18 keV mass) projected statistical upper limits (95) around  $10^{-7} |U_{e4}|^2$  (but will need detector upgrades)

in Project 8 measure the absolute neutrino mass using cyclotron radiation emission spectroscopy (CRES), may also be able to search for HNLs

atmospheric argon 39Ar: Q=565keV

DUNE: massive LArTPCs at long baseline (1300km) accelerator nu (1GeV), measure ionization charge of 39Ar beta decays: projected sensitivity in 20kev to 450keV mass range for  $|U_{e4}|^2$  at  $10^{-7}$  (requires substantial trigger development), without more like  $10^{-5}$

**Electron Capture** requires total energy-momentum reconstruction of non nu final states in electron capture

e capture: pure 2-body decay of recoiling atom and electron neutrino (mono energetic) measuring atom and associated de-excitation xray or auger electron, energy momentum conservation can be probed

separated non-zero missing mass peak would indicate HNL mixing with the electron neutrino/antineutrino

BeEST experiment: 100-850 keV mass, 7Be (Q=862keV), previous results at  $10^{-4} |U_{e4}|^2$ , future sensitivity at  $10^{-7} |U_{e4}|^2$  after upgrades to the experiment

(proposed) HUNTER experiment: 20-300 keV mass (K-capture of 131Cs), "significantly improve current limits"

**Reactor Searches** MeV masses (up to 12) at short baseline reactor experiments (commercial or research reactors)

source of electron antineutrinos, therefore also HNL (if they mix)

visible channels: N to nu e+ e-, and N to nu gamma, nu gamma gamma, where the first dominates

pioneering analysis reports  $10^{-4} |U_{e4}|^2$  at 2-7 MeV mass range

many experiments exist at 5-25 meters from reactor core, at 100 MW research or 1 GW commercial reactors and 1-5 m<sup>3</sup> volume detectors.. these are designed to address reactor anomaly, but could most likely also probe decay in flight to electron positron

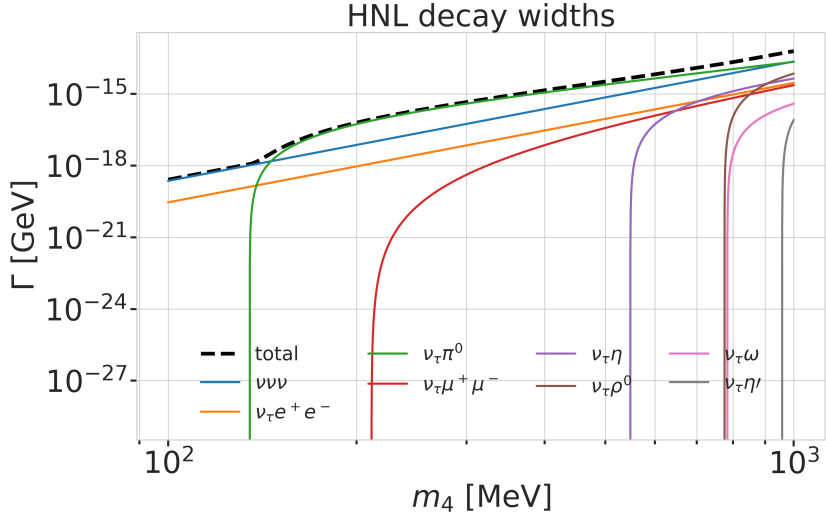


**Figure 1.2:** Decay widths of the HNL within the mass range considered, calculated based on the results from [20]. Given the existing constraints on  $|U_{e4}|^2$  and  $|U_{\mu 4}|^2$ , we consider that the corresponding decay modes are negligible.

### Extracted Beamlines

#### Atmospheric and Solar

#### Cosmological and Astrophysical

## 1.3 Atmospheric Neutrinos as Source of Heavy Neutral Leptons

write some interlude to motivate atm. neutrinos as source for HNL searches/production etc.

[16]: Tanabashi et al. (2018), “Review of Particle Physics”

### 1.3.1 Production of Neutrinos in the Atmosphere

The analysis performed in this work is based on the sample of neutrinos observed in IceCube DeepCore at energies below 100 GeV. At these energies, the flux exclusively originates in the Earth’s atmosphere. Highly relativistic cosmic rays (protons and heavier nuclei [16]) interact in the upper atmosphere, producing showers of secondary particles. Neutrinos are produced in decays of charged pions and kaons ( $\pi$  and  $K$  mesons) present in those showers, where the dominant contribution comes from the decay chain

$$\begin{aligned} \pi^\pm &\rightarrow \mu^\pm + \nu_\mu(\bar{\nu}_\mu), \\ \mu^\pm &\rightarrow e^\pm + \bar{\nu}_\mu(\nu_\mu) + \nu_e(\bar{\nu}_e), \end{aligned} \quad (1.18)$$

where muon neutrinos  $\nu_\mu$  and muons  $\mu^\pm$  are produced in the first decay and both electron and muon neutrinos  $\nu_{e/\mu}$  are produced in the second decay. Atmospheric muons, which are also produced in these decays, are the main background component for IceCube DeepCore analyses.

The different atmospheric flux components are shown in Figure 1.3 (left), for a much broader energy range than relevant for this work. Both neutrinos and antineutrino fluxes are shown for electron and muon neutrinos and all fluxes are the directionally averaged expectation calculated at the South Pole. Muon neutrinos are dominating the flux and from Equation 1.18 the naive assumption would be that the ratio between muon and electron neutrinos is  $(\nu_\mu + \bar{\nu}_\mu)/(\nu_e + \bar{\nu}_e) = 2$ . This is roughly true at energies below 1 GeV, where

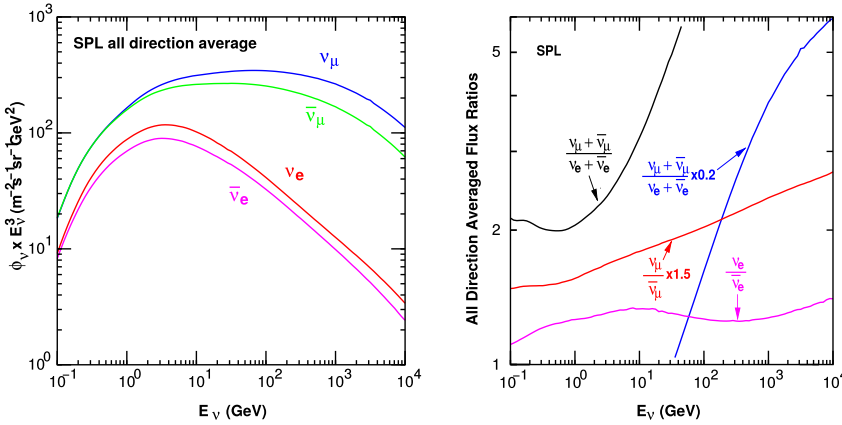


**Figure 1.3:** The atmospheric fluxes of different neutrino flavors as a function of energy (left) and the ratios between muon neutrinos and electron neutrinos as well as the ratios between neutrinos and antineutrinos for both those flavors (right). Results from the calculations performed for the geographic South Pole, taken from [21].

all muons decay in flight, but at larger energies muons can reach the detector before decaying, which increases the ratio to approximately 10:1 at around 100 GeV. Additionally, kaon decays start to contribute which also increases the number of muons and muon neutrinos. The increasing ratio can be seen in Figure 1.3 (right), which also shows the ratio between neutrinos and antineutrinos for both flavors.

Charged mesons or tau particles can also be produced in cosmic ray interactions. Their decays lead to the production of tau neutrinos. At the energies relevant for this work however, the resulting tau neutrino flux is negligible as compared to the muon neutrino flux [22] and is not considered in the analysis. This is because both charged mesons and tau particles are much heavier than pions and kaons and therefore their production is suppressed at high energies.

[22]: Fedynitch et al. (2015), “Calculation of conventional and prompt lepton fluxes at very high energy”

### 1.3.2 Interactions with Nuclei

The neutrino detection principle of IceCube DeepCore is explained in Chapter ?? and relies on the weak interaction processes between neutrinos and the nuclei of the Antarctic glacial ice. At neutrino energies above 5 GeV, the cross-sections are dominated by *deep inelastic scattering (DIS)*, where the neutrino is energetic enough to resolve the underlying structure of the nucleons and interact with one of the composing quarks individually. As a result the nucleon breaks and a shower of hadronic secondary particles is produced. Depending on the type of interaction, the neutrino either remains in the final state for NC interactions or is converted into its charged lepton counterpart for CC interactions. The CC DIS interactions have the form

$$\begin{aligned} \nu_l + N &\rightarrow l^- + X , \\ \bar{\nu}_l + N &\rightarrow l^+ + X , \end{aligned} \quad (1.19)$$

where  $\nu_l/\bar{\nu}_l$  and  $l^-/l^+$  are the neutrino/antineutrino and its corresponding lepton/antilepton, and  $l$  can be either an electron, muon, or tau.  $N$  is the nucleon and  $X$  stands for any set of final state hadrons. The NC DIS interactions are

$$\begin{aligned} \nu_l + N &\rightarrow \nu_l + X \text{ and} \\ \bar{\nu}_l + N &\rightarrow \bar{\nu}_l + X . \end{aligned} \quad (1.20)$$

Say something about atmospheric neutrino flux uncertainties, based on recent JP/Anatoli papers.

Figure 1.4 shows the Feynman diagrams for both processes DIS interactions

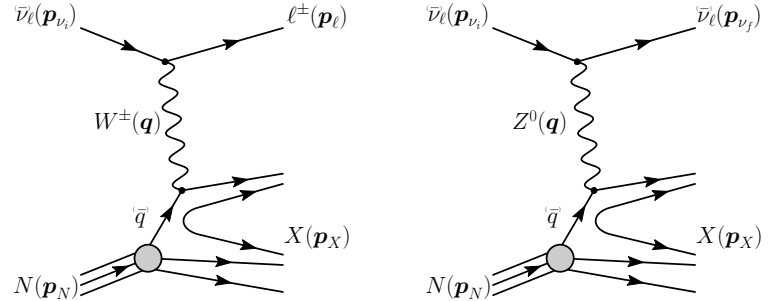


**Figure 1.4:** Feynman diagrams for deep inelastic scattering of a neutrino with a nucleon via charged-current (left) and neutral current (right) interactions.  $p_{\nu_i}$ ,  $p_N$  and  $p_{\nu_f}$ ,  $p_l$ ,  $p_X$  are the input and output four-momenta, while  $q$  is the momentum transfer. Taken from [11].

have a roughly linear energy dependent cross-section above  $\sim 20$  GeV and are well measured and easy to theoretically calculate. They are the primary interaction channel for neutrinos detected with IceCube.

At energies below 5 GeV, *quasi-elastic scattering (QE)* and *resonant scattering (RES)* become important. At these energies the neutrinos interact with the approximately point-like nucleons, without breaking them up in the process. RES describes the process of a neutrino scattering off a nucleon producing an excited state of the nucleon in addition to a charged lepton. It is the dominant process at 1.5 GeV to 5 GeV for neutrinos and 1.5 GeV to 8 GeV for antineutrinos. Below 1.5 GeV QE is the main process, where protons are converted to neutrons in antineutrino interactions and vice-versa for neutrino interactions. Additionally, a charged lepton corresponding to the neutrino/antineutrino flavor is produced. The cross-sections of QE and RES scattering processes are not linear in energy and the transition region from QE/RES to DIS is poorly understood. The total cross-sections and their composition is shown in Figure 1.5. It can be seen that the interaction cross-sections are very small at the order of  $10^{-38}$  cm $^2$ . This is the reason why very large volume detectors are required to measure atmospheric neutrinos with sufficient statistics to perform precision measurements of their properties. The interaction length of a neutrino with  $E_\nu = 10$  GeV is of  $\mathcal{O}(10 \times 10^{10}$  km), for example.

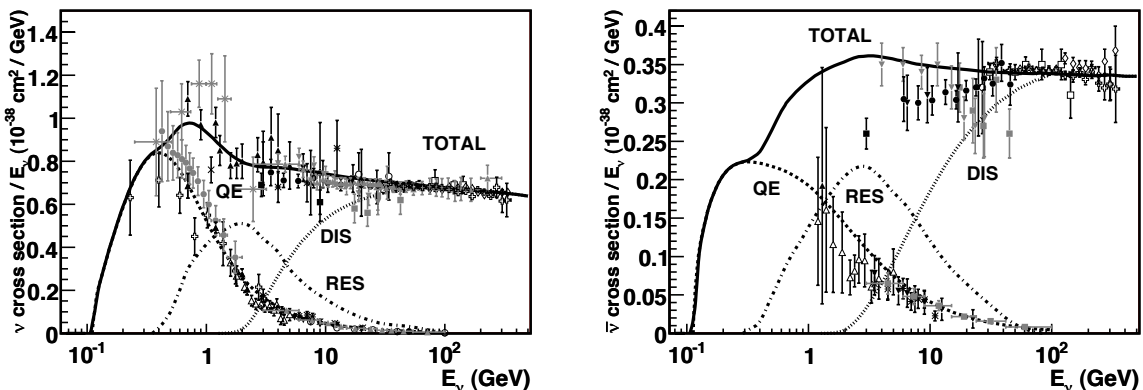


**Figure 1.5:** Total neutrino (left) and antineutrino (right) per nucleon cross-section divided by neutrino energy plotted against energy. The three main scattering processes quasi-elastic scattering (QE), resonant scattering (RES), and deep-inelastic scattering (DIS) are shown. Taken from [23].

### 1.3.3 Oscillations

So far we have described neutrinos in their flavor eigenstates, which are relevant for weak interactions. In the SM three-neutrino model the weak flavor states are  $\nu_e$ ,  $\nu_\mu$ , and  $\nu_\tau$ , which relate them to the charged leptons they interact with in CC interactions. There is a second way of describing neutrino wave functions based on their Hamiltonian eigenvalues [24], namely as the mass eigenstates  $\nu_1$ ,  $\nu_2$ , and  $\nu_3$ . These states are related to the flavor eigenstates by the unitary, 3x3 *Pontecorvo-Maki-Nakagawa-Sakata (PMNS)* matrix  $U$ , where the flavor states are a superposition of the mass states as

$$|\nu_\alpha\rangle = \sum_k U_{\alpha k}^* |\nu_k\rangle , \quad (1.21)$$

with the weak flavor states  $|\nu_\alpha\rangle$ ,  $\alpha = e, \mu, \tau$ , and the mass states  $|\nu_k\rangle$  with  $k = 1, 2, 3$ . The mixing matrix can be parameterized as [16]

$$U = \begin{pmatrix} 1 & 0 & 0 \\ 0 & c_{23} & s_{23} \\ 0 & -s_{23} & c_{23} \end{pmatrix} \begin{pmatrix} c_{13} & 0 & s_{13}e^{-i\delta_{CP}} \\ 0 & 1 & 0 \\ -s_{13}e^{i\delta_{CP}} & 0 & c_{13} \end{pmatrix} \begin{pmatrix} c_{12} & s_{12} & 0 \\ -s_{12} & c_{12} & 0 \\ 0 & 0 & 1 \end{pmatrix} , \quad (1.22)$$

where  $c_{ij} = \cos \theta_{ij}$  and  $s_{ij} = \sin \theta_{ij}$  are cosine and sine of the mixing angle  $\theta_{ij}$ , that defines the strength of the mixing between the mass eigenstates  $i$  and  $j$ , and  $\delta_{CP}$  is the neutrino CP-violating phase.

Describing neutrinos in their mass state is crucial to understand their propagation through space and time. Their propagation in vacuum can be expressed by applying a plane wave approach, where the mass eigenstates evolve as

$$|\nu_k(t)\rangle = e^{-iE_k t/\hbar} |\nu_k\rangle . \quad (1.23)$$

The energy of the mass eigenstate  $|\nu_k\rangle$  is  $E_k = \sqrt{\vec{p}^2 c^2 + m_k^2 c^4}$ , with momentum  $\vec{p}$  and mass  $m_k$ ,  $\hbar$  is the reduced Planck constant, and  $c$  is the speed of light in vacuum. The existence of non-zero, non-equal masses and the neutrino mixing relation in Equation 1.21, lead to the observed phenomenon of neutrino oscillations. Oscillations mean that a neutrino changes from its initial flavor, that it was produced with, to another flavor and back after traveling a certain distance. A neutrino is produced as a flavor eigenstate  $|\nu_\alpha\rangle$  in a CC weak interaction, but its propagation happens as the individual mass states it is composed of. The probability of finding the neutrino with initial flavor  $|\nu_\alpha\rangle$  in the flavor state  $|\nu_\beta\rangle$  after the time  $t$  is calculated as

$$P_{\nu_\alpha \rightarrow \nu_\beta}(t) = |\langle \nu_\beta | \nu_\alpha(t) | \nu_\beta | \nu_\alpha(t) \rangle|^2 , \quad (1.24)$$

by applying Fermi's Golden Rule [25], which defines the transition rate from one eigenstate to another by the strength of the coupling between them. This coupling strength is the square of the matrix element and using the fact that the mixing matrix is unitary ( $U^{-1} = U^\dagger$ ) to describe the mass eigenstates as flavor eigenstates, we find the time evolution of the flavor state  $|\nu_\alpha(t)\rangle$ , which can be inserted into Equation 1.24 to find the probability as

$$P_{\nu_\alpha \rightarrow \nu_\beta}(t) = \sum_{j,k} U_{\beta j}^* U_{\alpha j} U_{\beta k} U_{\alpha k}^* e^{-i(E_k - E_j)t/\hbar} . \quad (1.25)$$

The indices  $j$  and  $k$  run over the mass eigenstates. We can approximate the

[24]: Bilenky et al. (1978), "Lepton mixing and neutrino oscillations"

[16]: Tanabashi et al. (2018), "Review of Particle Physics"

add current BF values  
from nufit or so?

[25]: Dirac (1927), "The Quantum Theory of the Emission and Absorption of Radiation"

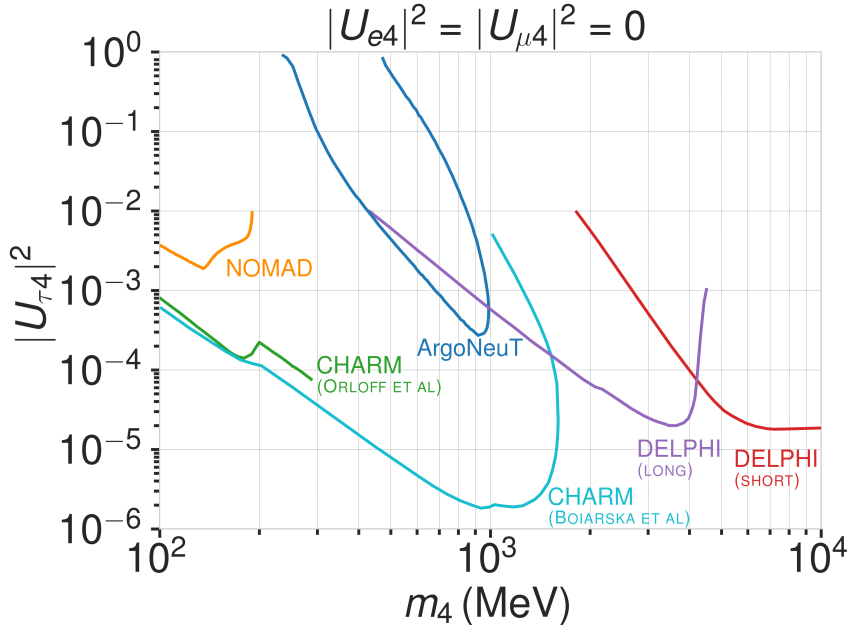


**Figure 1.6:** Current  $|U_{\tau 4}^2| - m_4$  limits from NOMAD [27], ArgoNeut [28], CHARM [29, 30], and DELPHI [31].

energy as

$$E_k \approx E + \frac{c^4 m_k^2}{2E} \quad \rightarrow \quad E_k - E_j \approx \frac{c^4 \Delta m_{kj}^2}{2E}, \quad (1.26)$$

for small neutrino masses compared to their kinetic energy. Here,  $\Delta m_{kj}^2 = m_k^2 - m_j^2$  is the mass-squared splitting between states  $k$  and  $j$ . Replacing the time in Equation 1.25 by the distance traveled by relativistic neutrinos  $t \approx L/c$  we get

$$\begin{aligned} P_{\nu_\alpha \rightarrow \nu_\beta}(t) &= \delta_{\alpha\beta} - 4 \sum_{j>k} \operatorname{Re}(U_{\beta j}^* U_{\alpha j} U_{\beta k} U_{\alpha k}^*) \sin^2\left(\frac{c^3 \Delta m_{kj}^2}{4E\hbar} L\right) \\ &\quad + 2 \sum_{j>k} \operatorname{Im}(U_{\beta j}^* U_{\alpha j} U_{\beta k} U_{\alpha k}^*) \sin^2\left(\frac{c^3 \Delta m_{kj}^2}{4E\hbar} L\right), \end{aligned} \quad (1.27)$$

which is called the survival probability if  $\alpha = \beta$ , and the transition probability if  $\alpha \neq \beta$ . Once again, this probability is only non-zero if there are neutrino mass eigenstates with masses greater than zero. Additionally, there must be a mass-squared difference  $\Delta m^2$  and non-zero mixing between the states. Since we assumed propagation in vacuum in Equation 1.23, the transition and survival probabilities correspond to vacuum mixing.

say something about how this changes with matter

### 1.3.4 Testing Heavy Neutral Leptons with Atmospheric Neutrinos

Re-write/re-formulate this section (copied from HNL technote).

[26]: Yanagida (1980), "Horizontal Symmetry and Masses of Neutrinos"

Produce similar styled plot for these limits

#### The Minimal Standard Model Extension

Extensions to the Standard Model (SM) that add *Heavy Neutral Leptons* (HNLs) provide a good explanation for the origin of neutrino masses through different seesaw mechanisms [26]. While the mixing with  $\nu_e/\mu$  is strongly constrained ( $|U_{\alpha 4}^2| \lesssim 10^{-5} - 10^{-8}$ ,  $\alpha = e, \mu$ ), the mixing with  $\nu_\tau$  is much harder to probe due to the difficulty of producing and detecting  $\nu_\tau$ . Figure

1.6 shows the current limits on the  $\tau$ -sterile mixing space for HNL masses between 0.1 GeV-10 GeV. As was first pointed out in [32], the atmospheric neutrino flux observed in IceCube offers a way to constrain the neutrino-HNL mixing parameters. By using the large fraction of atmospheric  $\nu_\mu$  events that oscillate into  $\nu_\tau$  before they reach the detector, the less constrained  $\tau$ -sterile mixing space can be explored. In this document, we present the methodology and strategy of a search for HNLs with IceCube DeepCore. These additional RH neutrinos can be included in the Standard Model (SM) by extending the PMNS matrix to at least a 3x4 matrix as

$$\begin{pmatrix} \nu_e \\ \nu_\mu \\ \nu_\tau \\ \nu_s \end{pmatrix} = \begin{pmatrix} U_{e1} & U_{e2} & U_{e3} & U_{e4} \\ U_{\mu 1} & U_{\mu 2} & U_{\mu 3} & U_{\mu 4} \\ U_{\tau 1} & U_{\tau 2} & U_{\tau 3} & U_{\tau 4} \\ U_{s1} & U_{s2} & U_{s3} & U_{s4} \end{pmatrix} \begin{pmatrix} \nu_1 \\ \nu_2 \\ \nu_3 \\ \nu_4 \end{pmatrix}, \quad (1.28)$$

where the components with index 4 define the mixing between the flavor states and the fourth sterile mass state, respectively. Note here that this is not a theoretically fully consistent picture, but rather the phenomenologically minimal model to be tested by this analysis. This can hopefully be put into the larger context of several fully consistent models, later. Due to the singlet nature of the RH neutrinos, they only interact weakly, inheriting these interactions from their LH neutrino counterparts via mixing. This mixing of the HNLs with the electron, muon, and tau neutrinos can be probed and constrained as a function of the HNL mass by searching for their production and decay. In [32, 33] this search is mainly motivated through two experimental arguments. Secondly, IceCube is ideally placed to explore the yet unconstrained  $|U_{\tau 4}|^2 - m_4$  phase-space that is not easily accessible by accelerator-based experiments.

In order to probe the  $\tau$ -sterile mixing parameter, it is required to look at interactions involving  $\tau$  neutrinos. However, most neutrinos produced in cosmic ray interactions with the atmosphere are  $\nu_e$  or  $\nu_\mu$ . Therefore, we need these neutrinos to oscillate to the  $\tau$  flavor before reaching the detector. For this to happen at the considered energies a traveled distance of the order of the earth diameter is necessary. This is why our signal is mostly up-going and passing through the whole earth.

To explain the signature we can observe in IceCube we first have to revisit the weak interactions that the HNL inherits from its LH counterpart through mixing. We will be following the derivation in [20]. Extending the SM by  $n$  additional RH neutrinos,  $\nu_i$  ( $i = 3 + n$ ), leads to the mass Lagrangian

$$\mathcal{L}_\nu^{\text{mass}} \supset - \sum_{\alpha=e,\mu,\tau} \sum_{i=4}^{3+n} Y_{\nu,\alpha i} \bar{L}_{L,\alpha} \tilde{\phi} \nu_i - \frac{1}{2} \sum_{i=4}^{3+n} M_i \bar{\nu}_i \nu_i^c + h.c., \quad (1.29)$$

in a basis where the Majorana mass terms are diagonal.  $Y_{\nu,\alpha i}$  are the Yukawa couplings to the lepton doublets and  $M$  the Majorana masses for the heavy singlets.  $L_{L,\alpha}$  stands for the SM LH lepton doublet of flavor  $\alpha$  while  $\phi$  is the Higgs field, and  $\tilde{\phi} = i\sigma_2\phi^*$  and  $\nu_i^c \equiv C\bar{\nu}_i^t$ , with  $C = i\gamma_0\gamma_2$  in the Weyl representation. The full neutrino mass matrix with the Higgs vacuum expectation value  $v/\sqrt{2}$  reads

$$\mathcal{M} = \begin{pmatrix} 0_{3 \times 3} & Y_\nu v / \sqrt{2} \\ Y_\nu^t v / \sqrt{2} & M \end{pmatrix}, \quad (1.30)$$

[32]: Coloma et al. (2017), "Double-Cascade Events from New Physics in Icecube"

[32]: Coloma et al. (2017), "Double-Cascade Events from New Physics in Icecube"

[33]: Coloma (2019), "Icecube/DeepCore tests for novel explanations of the MiniBooNE anomaly"

This section really needs to be re-written to motivate the search for HNLs from a more generic point of view (e.g. to explain neutrino masses)

This section definitely needs to be elaborated in a little more detail

[20]: Coloma et al. (2021), "GeV-scale neutrinos: interactions with mesons and DUNE sensitivity"

Not adding information about the case where the neutrinos have Dirac or pseudo-Dirac masses

and can be diagonalized by a  $(3+n) \times (3+n)$  full unitary rotation  $U$ , that itself leads to neutrino masses upon diagonalization, additionally manifesting the mixing between active neutrinos and heavy states. The resulting model consists of 3 light SM neutrino mass eigenstates  $\nu_i$  ( $i = 1, 2, 3$ ) and  $n$  heavier states, as introduced above. The flavor states will now consist of a combination of light and heavy states

$$\nu_\alpha = \sum_{i=1}^{3+n} U_{\alpha i} \nu_i, \quad (1.31)$$

and the leptonic part of the EW Lagrangian can be written as

$$\begin{aligned} \mathcal{L}_{EW}^\ell = & \frac{g}{\sqrt{2}} W_\mu^+ \sum_\alpha \sum_i U_{\alpha i}^* \bar{\nu}_i \gamma^\mu P_L \ell_\alpha + \frac{g}{4c_w} Z_\mu \\ & \times \left\{ \sum_{i,j} C_{ij} \bar{\nu}_i \gamma^\mu P_L \nu_j + \sum_\alpha \bar{\ell}_\alpha \gamma^\mu [2s_w^2 P_R - (1-2s_w^2) P_L] \ell_\alpha \right\} + h.c., \end{aligned}$$

where  $c_w \equiv \cos \theta_w$ ,  $s_w \equiv \sin \theta_w$ , and  $\theta_w$  the SM weak mixing angle or *Weinberg angle*.  $P_L$  and  $P_R$  are the left and right projectors, respectively, while

$$C_{ij} \equiv \sum_\alpha U_{\alpha i}^* U_{\alpha j}. \quad (1.32)$$

The indices now sum over all  $(3+n)$  flavor and mass states.

Based on this formulation and assuming that only the mixing with the tau sector is open ( $|U_{\alpha 4}|^2 = 0$ ,  $\alpha = e, \mu$ ), the relevant production diagram of the HNL can be drawn as shown in Figure 1.7. Alongside the fourth heavy mass state, a Hadronic cascade is produced. The heavy mass state will travel for some distance (dependent on mass and mixing) before it decays. The subsequent decay processes are depicted in Figure 1.8. It can be a CC or NC decay and both leptonic and mesonic modes are possible (dependent on the mass). This will produce a tau or a tau neutrino and another cascade that can be EM or Hadronic. The branching ratios corresponding to the decay modes of the HNL for the mass range of interest (i.e. between 100 MeV and 1 GeV) are shown in Figure 1.9a as a function of the HNL mass.

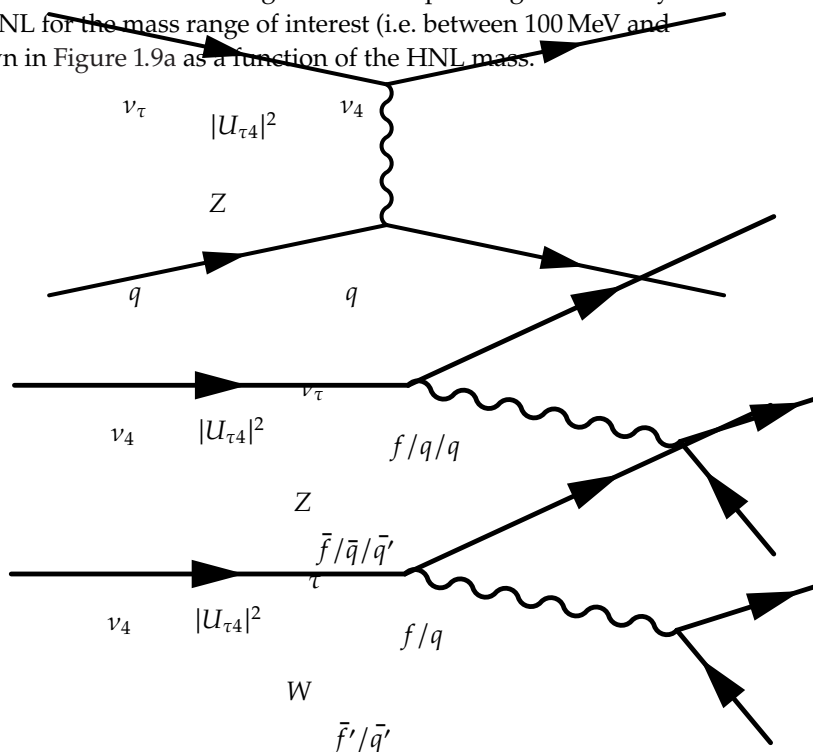


**Figure 1.7:** Production of a sterile neutrino in the up-scattering of a tau neutrino.

**Figure 1.8:** Sterile neutrino decay through neutral current (left) and charged current (right).

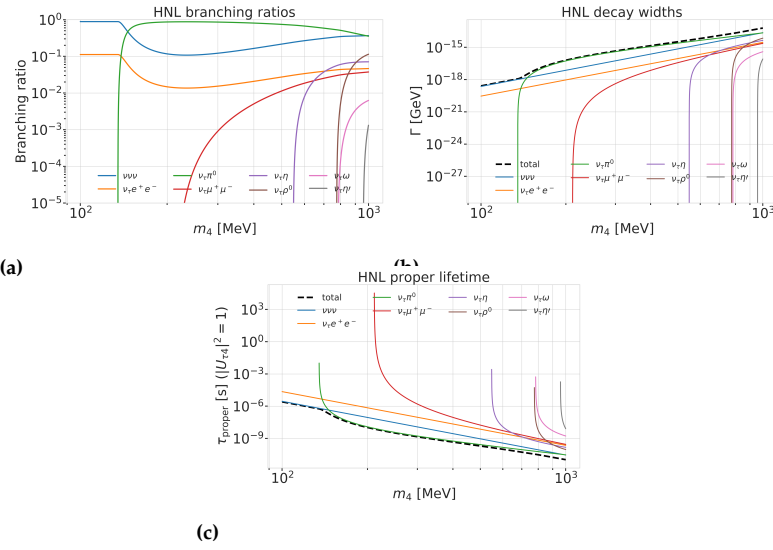


**Figure 1.9:** Branching ratios, decay widths, and proper lifetime of the HNL within the mass range considered, calculated based on the results from [20].

### Production and Decay in IceCube DeepCore



# Detecting Low Energetic Double Cascades

# 2

## 2.1 Reconstruction

All existing reconstruction algorithms applied for low energetic atmospheric neutrino events mentioned in Section ?? are either assuming a single cascade hypothesis or a track and cascade hypothesis, which are the two SM morphologies observable at these energies, as was described in Section ?? . A HNL being produced and decaying inside the IceCube detector however, will produce two cascade like light depositions. The morphology and how the cascade properties and their spatial separation depend on the model parameters was introduced in Section 1.3.4. To investigate the performance of the detector to observe these events, a low energetic double cascade reconstruction algorithm was developed, based on a pre-existing algorithm used to search for double cascades produced from high energetic astrophysical tau neutrinos [34] that was established in [35], but first mentioned in [36].

### 2.1.1 Table-Based Minimum Likelihood Algorithms

The reconstruction is relying on a maximum likelihood algorithm, which is the *classical* approach to IceCube event reconstructions, as opposed to ML based methods. A Poissonian likelihood is constructed, which compares the observed photon numbers,  $n$ , with their arrival times to the expected light depositions,  $\mu$ , for a given even hypothesis as

$$\ln(L) = \sum_j \sum_t n_{j,t} \cdot \ln(\mu_{j,t}(\Theta) + \rho_{j,t}) - (\mu_{j,t}(\Theta) + \rho_{j,t}) - \ln(n_{j,t}!) , \quad (2.1)$$

where  $\rho$  are the number of expected photons from noise,  $\Theta$  are the parameters governing the source hypothesis, and the likelihood is calculated summing over all DOMs  $j$  splitting observed photons into time bins  $t$ . The light expectations are calculated using look-up tables [37] that contain the results from MC simulations of reference cascade events or track segments. By varying the parameters defining the event hypothesis, the likelihood of describing the observed light pattern by the expected light depositions is maximized to find the reconstructed event. Algorithms of this kind used in IceCube are described in great detail in [38]. For the table production a specific choice of ice model has to be made, while the calibrated DOM information is taken from the measurement itself.

Based on the tabulated light expectations for cascades and track segments, various event hypothesis can be constructed, like the common cascade only or the track and cascade hypotheses. The hypothesis describing the double cascade signature of the HNL is using two reference cascades that are separated by a certain distance. The whole hypothesis is defined by 9 parameters and assumes that the two cascades are aligned with each other, which is a safe assumption for strongly forward boosted interactions. The parameters are the position of the first cascade  $x, y, z$ , the direction of both cascades  $\phi, \theta$ , and its time  $t$  as well as the decay length  $L$  between the

2.1	Reconstruction	17
2.2	Double Cascade Classification	24
2.3	Generic Double Cascade Performance	24

[34]: Abbasi et al. (2020), "Measurement of Astrophysical Tau Neutrinos in IceCube's High-Energy Starting Events"

[35]: Usner (2018), "Search for Astrophysical Tau-Neutrinos in Six Years of High-Energy Starting Events in the IceCube Detector"

[36]: Hallen (2013), "On the Measurement of High-Energy Tau Neutrinos with IceCube"

maybe I want a figure for this, or not so important? (YELLOW)

[37]: Whitehorn et al. (2013), "Penalized splines for smooth representation of high-dimensional Monte Carlo datasets"

[38]: Aartsen et al. (2014), "Energy Reconstruction Methods in the IceCube Neutrino Telescope"

Elaborate whether this is the case (show it in a plot?). Discuss directionality of cascades in general. (ORANGE)

two cascades. Assuming the speed of the HNL to be the speed of light,  $c$ , this already defines the full signature. The HNL particle does not produce any light while traveling, as it is electrically neutral. The full 9 parameters describing the event are  $\Theta = (x, y, z, t, \theta, \phi, E_0, E_1, L)$ . To compute the full likelihood the term in Equation 2.1 is summed over both cascade parts,  $i$ , as  $\sum_i \ln(L_i)$ .

### 2.1.2 Optimization for Low Energy Events

Optimizing the double cascade reconstruction for low energetic events was done in parallel to the development of the model dependent simulation generator introduced in Section ???. A preliminary sample of HNL events was used, containing a continuum of masses between 0.1 GeV and 1.0 GeV and lab frame decay lengths sampled uniformly in the range from 5 m to 500 m. Even though this sample is not representative of a physically correct model and therefore not useful to predict the event expectation, it can still be used to optimize the reconstruction. The double cascade nature of the individual events and the evenly spaced decay length distribution are especially useful for this purpose.

The simulation is processed up to Level 5 of the selection chain described in Section ?? and one of the reconstructions from [39] is applied to the events, fitting a cascade and a track and cascade hypothesis. The results from this reconstruction are used as an input for the double cascade reconstruction, where the position of the vertex, the direction of the event, and its interaction time are used as the input quantities for the first cascade, and the length of the track reconstruction is used as a seed for the distance between the two cascades.

#### Decay Length Seeds

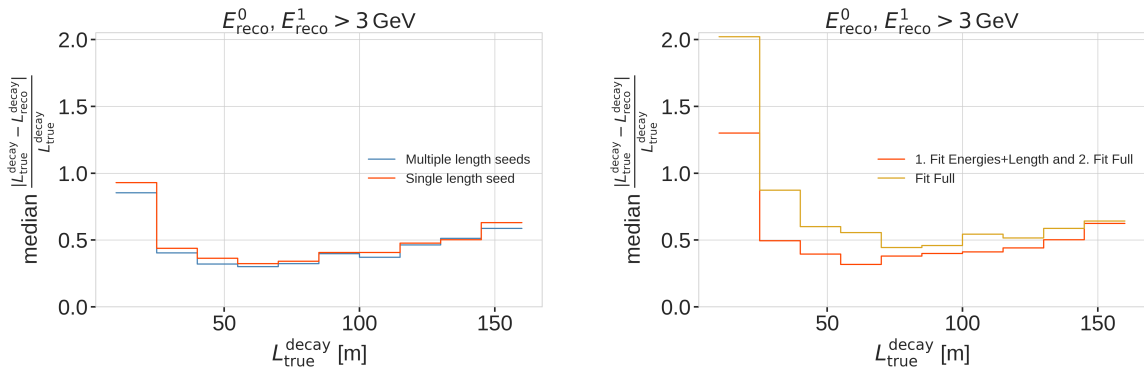


**Figure 2.1**

fix caption of this figure  
(RED)

The full 9 dimensional likelihood space is very complex and can have many local minima, depending on the specific event and its location in the detector. Especially the seed value of the length between the two cascades was found to have a very strong impact on whether the global minimum was found during the minimization. To mitigate this effect, multiple fits are performed, seeding with variations of the input length at different orders of magnitude. The best result is used, selected based on the total likelihood value of the

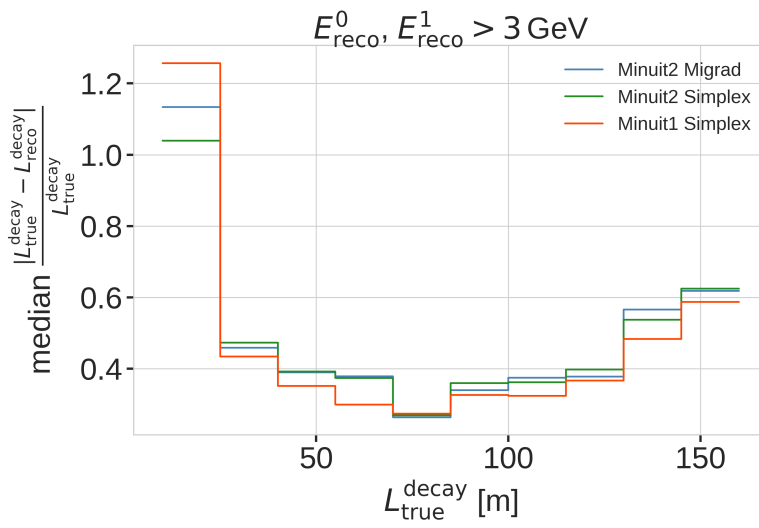
best fit parameter set. A small improvement in the decay length resolution can be found by using this approach as compared to a single length seed. The effect can be seen in the left part of Figure 2.1, which shows the median, absolute, fractional decay length resolution.

### Fit Routine

Because the length seed showed to have such a large impact on the reconstruction performance, a more sophisticated fit routine, than just fitting all 9 parameters at once, was tested. In a first fit iteration, some parameters are fixed and the resulting best fit point is used to fit all 9 parameters in a second iteration. In the right part of Figure 2.1 it can be seen how a fit split into two consecutive steps, where the first step fits only both cascade energies and the decay length and the second step fits the full 9 parameters, performs better as compared to a single, full 9 parameter fit. The initial seed for both routines is the same.

### Minimizer Settings

To investigate the effect of the minimizer used to find the best fit parameters, the reconstruction was performed using three different minimizers, which were easily accessible within the reconstruction framework. The minimizers used were Minuit1 Simplex, Minuit2 Simplex, and Minuit2 Migrad. The results can be seen in Figure 2.2, where the Minuit1 Simplex minimizer performs best. The initial idea was to test a global minimizer, or a routine that can find the rough position of the global minimum first and then a local minimizer to find the exact minimum, but unfortunately this was not possible with the minimizers available in the framework. From the three tested minimizers, Minuit1 Simplex performed best and was chosen as the default for the reconstruction. The comparison of the decay length resolutions can be seen in Figure 2.2.



fix caption of this figure  
(RED)  
Figure 2.2: title

### 2.1.3 Performance

The chosen reconstruction chain used to test the performance of the detector to observe low energetic double cascades is the following; Minuit1 Simplex is used as the minimizer, the decay length is seeded with 3 different values, 0.5x, 1.0x, and 1.5x the length of the track reconstruction, and the fit routine is split into two steps, where the first step fits the energies and the decay length and the second step fits the full 9 parameters. In the first step, the number of time bins in Equation 2.1 is set to 1, so just the number of photons and their spatial information is used. The second step is seeded with the best results from the first fit and here the number of time bins is chosen such that each photon falls into a separate time bin, which means all time information is used. The average runtime per event is  $\sim 16$  s on a single CPU core, but is very dependent on the number of photons observed in the event, since the likelihood calculation in the second step scales with this number and a table lookup has to be performed for each photon.

To get a more realistic estimate of the reconstruction performance, it is run on a second preliminary sample of HNL events, containing masses between 0.1 GeV and 3.0 GeV and the lab frame decay length is sampled from an inverse distribution in the range from 1 m to 1000 m, which is a better approximation of the expected exponential decay distribution of the HNL. The performance is shown for events where the reconstruction chain was successfully run, the event selection criteria up to level 7 are fulfilled, and the reconstructed energy of both cascades is above 3.0 GeV. This is done to only investigate well reconstructed events with two significant light depositions at a usual final selection level of the oscillation analyses.

one half sentence on why  
this number was chosen?  
(ORANGE)

### Energy Resolutions

The energy resolution is inspected by looking at the 2-dimensional distribution of reconstructed energy versus the true energy as shown in Figure 2.3. The bin entries are shown as well as the median and  $\pm 25\%$  calculated per vertical column, to get an idea of the distribution for a given energy slice. The color scale is showing the PDF along in each true energy slice, which is the full information combined into the median $\pm 25\%$  lines. The reconstructed energy is only the energy that is observable from photons, while the true energy is the total cascade energy, including the parts that go into EM neutral particles that do not produce light. It is therefore not expected that the median lines up with the axis diagonal, but rather the reconstructed energy is going to be lower.

The histogram for the first cascade energy is shown on the left and above an energy of  $\sim 10$  GeV the reconstruction performs well, with the median being parallel to the diagonal and the spread in the  $\pm 25\%$  quantile being small. Below this energy the reconstruction is over-estimating the true energy, which is a known effect in IceCube, where the reconstruction is biased towards higher energies around the energy detection threshold, because events that enter the sample are events with an over fluctuation in their light deposition, which makes them pass into the selection and being reconstructible in the first place.

For the second cascade the overall behavior is similar, only that the energy where the reconstruction starts to perform good is higher around  $\sim 20$  GeV.

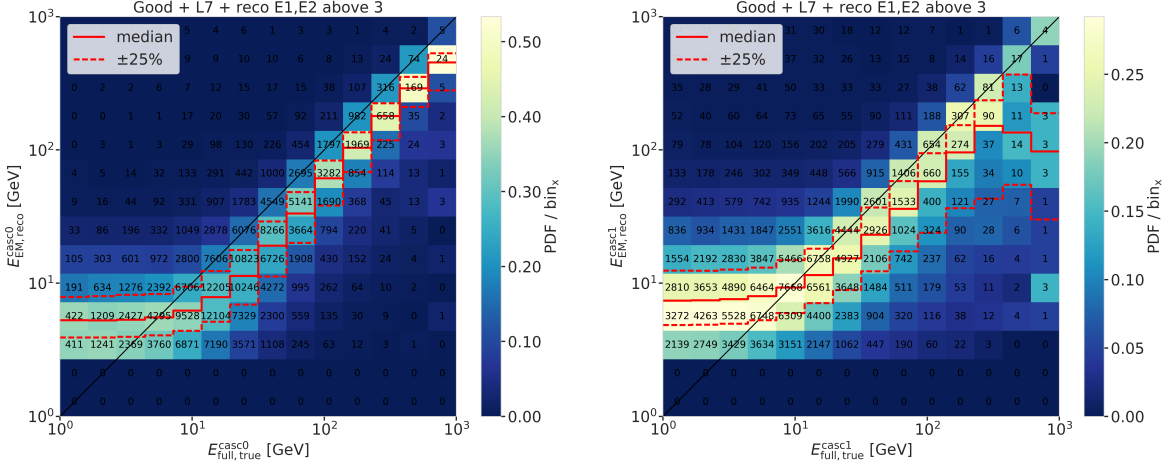


**Figure 2.3:** Reconstructed (EM) energy versus true energy (full) energy for the first cascade (left) and second cascade (right). The color scale is according to the PDF in each vertical true energy slice, with the solid and dashed lines showing the median $\pm 25\%$  quantiles. The bin entries are shown as numbers.

The spread around the median is also larger and starts to expand a lot above 200 GeV, where the statistics are lower as can be seen from the bin counts. It is also very apparent that the majority of energies of the second cascade are at lower true energy values between 1 GeV and 20 GeV.

For both cascade resolutions the effect of the reconstruction being biased towards lower values, due to the comparison of the full true energy to the reconstructed EM energy can be seen.

### Length Resolutions

The decay length resolution is also investigated by looking at a similar style of 2-d histograms as for the energies, where the reconstructed decay length is plotted versus the true decay length. The left part of Figure 2.4 shows the distributions after the same selection criteria from Section 2.1.3 are applied. It can be observed that for short true lengths the reconstruction is over-estimating the length, while for long true lengths the reconstruction is strongly under-estimating the length. There is a region between true lengths of 20 m and 80 m where the median reconstruction is almost unbiased, but the 50 % interquartile range is large and increasing from  $\sim 50$  m to  $\sim 70$  m with true decay lengths.

The over-estimation at small true lengths can be explained for multiple reasons, one being that the shortest DOM spacing is  $\sim 7$  m, vertically for DeepCore strings, but mostly larger than that, so resolving lengths below this is very complicated, and the reconstruction tends to be biased towards estimating the length around where the light was observed. Another reason is a similar argument to why the energies are over-estimated at small true values, namely that events that passed the selection and were reconstructed in those cases, probably have an over fluctuation in light deposition, extending further out from the vertices, so the reconstructed length is larger. Additionally, approaching a length of 0.0, the reconstructed length will of course always be a one-sided distribution, because the lengths have to be positive.

The under-estimation at large true lengths is more puzzling, and it seems like the distribution becomes bimodal in the reconstructed lengths, with

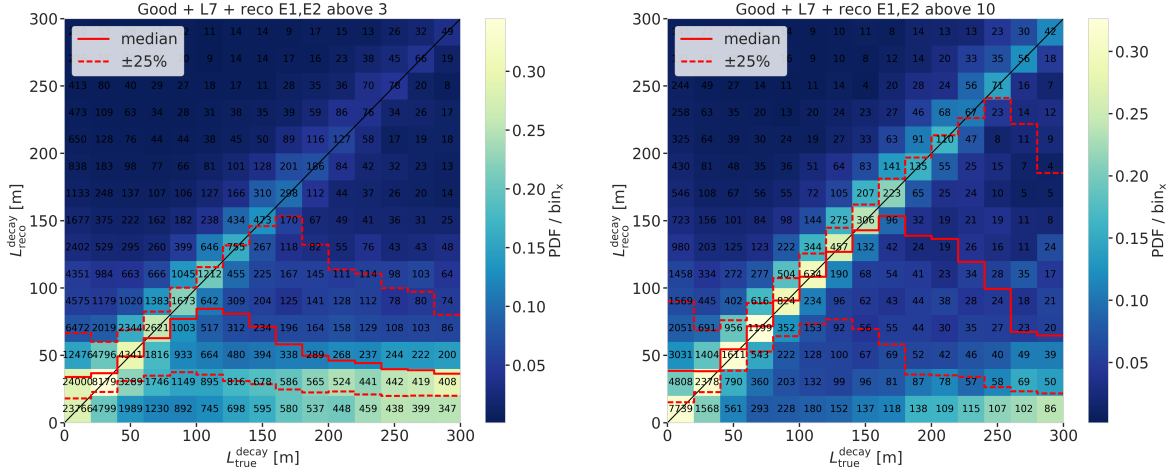


**Figure 2.4:** Reconstructed decay length versus true decay length for  $\sim 3\text{ GeV}$  (left) and  $\sim 10\text{ GeV}$  (right) minimum reconstructed cascade energies. The color scale is according to the PDF in each vertical true length slice, with the solid and dashed lines showing the median  $\pm 25\%$  quantiles. The bin entries are shown as numbers.

one population around the diagonal, meaning that they are properly reconstructed, and one population at very short reconstructed lengths, which are badly reconstructed. Above 150 m the badly reconstructed population starts to dominate, and the median resolution drops off strongly. The assumption is that for these events, only one cascade was observed with enough light to be reconstructed, and the reconstruction describes the one observed cascade in two parts, separated by a short distance, driven by similar factors as mentioned before. A quick check to confirm whether this is the case, was to increase the selection criteria to minimum reconstructed cascade energies of 10 GeV, which is shown in the right part of Figure 2.4. It can be seen that the median resolution is already much better, aligning with the expectation between 40 m and 160 m. Judging from the median resolution and the  $+25\%$  quantile in this range, there is very few events with an over-expectation in the energy, since both of them are alidgning with the diagonal. The spread towards lower reconstructed lengths, on the other hand, is still very large and above 200 m the badly reconstructed population starts to dominate again.

#### Badly Reconstructed Cascade Population

make on figure, where  
the two selected regions  
are highlighted? (RED)

fix caption (RED)

To investigate the badly reconstructed population further, a rough separation was made to find out what the cause of the difference is. It was already established that a larger reconstructed energy in both cascades, which is related to a larger true energy in form of more deposited light, leads to a better reconstruction in more events. As shown in Figure 2.5, only events with true decay length larger than 80 m are used, where the populations are split by the reconstructed decay length being larger or smaller than 80 m. Based on a few potential sourced of bad reconstruction, several variables were checked to see if there is a difference between the two populations.

The left part of Figure 2.6 shows the true horizontal distance of the second cascade from string 36. The distance is denoted as  $\rho_{36}$  and is a very good proxy for the distance to the center of the detector, because string 36 is almost at the center. While the distributions looks very similar for the first cascade

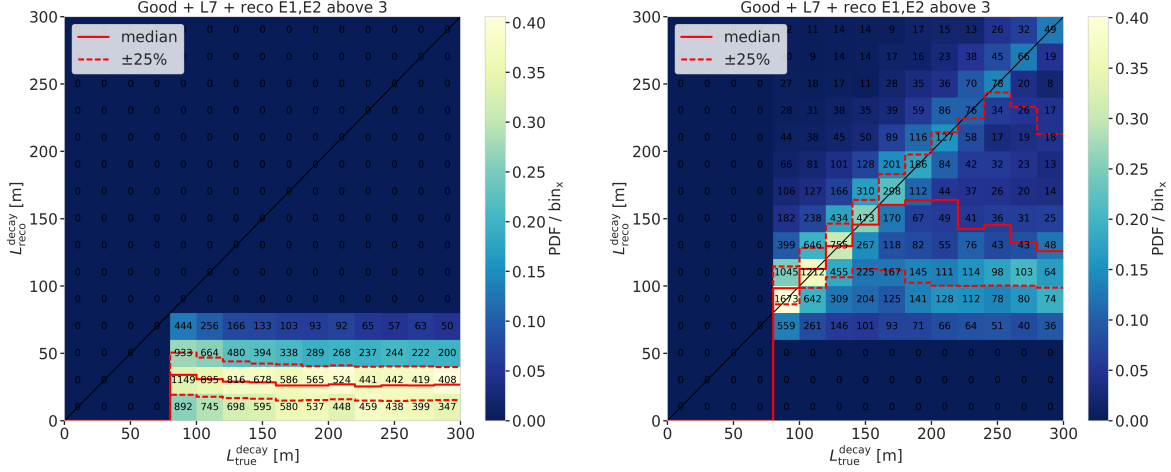


**Figure 2.5**

(not shown), for the second cascade the badly reconstructed population extends to larger values. Considering that the DeepCore strings are roughly inside a 70 m radius from the center, and the next layer of IceCube strings is at a radius of 125 m, this is a plausible explanation for a worse reconstruction, because for the badly reconstructed population the second cascades are more often in regions without DOMs, so less or no light is observed from them.

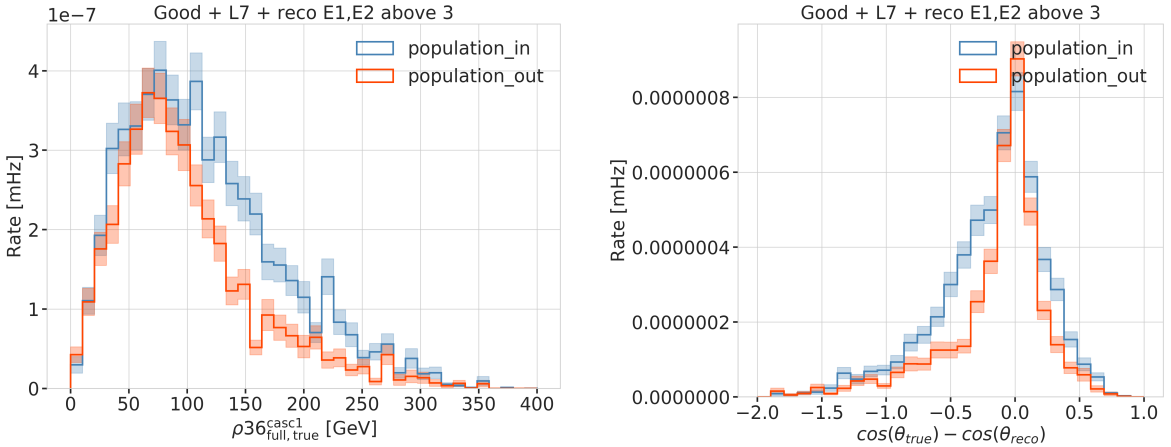


**Figure 2.6**

Another possible reason why the reconstruction underperforms could be that the initial seed direction was off and therefore one of the cascades cannot be found properly. Looking at the error of the cosine of the reconstructed zenith angle shown in the right of Figure 2.6, we see that the badly reconstructed population has a larger error, and is less peaked around 0.0. This could be a hint that the direction is worse for the badly reconstructed population, which could be due to a bad seed direction, or just the result of one cascade not being observed properly.

re-make normalized?  
(ORANGE)

fix caption (RED)

The true energies of both cascades are shown in Figure 2.5, where it can be observed that the first cascade energy is generally much larger than the second, peaking between 10 GeV and 20 GeV, while the second cascade peaks

re-make normalized?  
(ORANGE)

fix caption (RED)

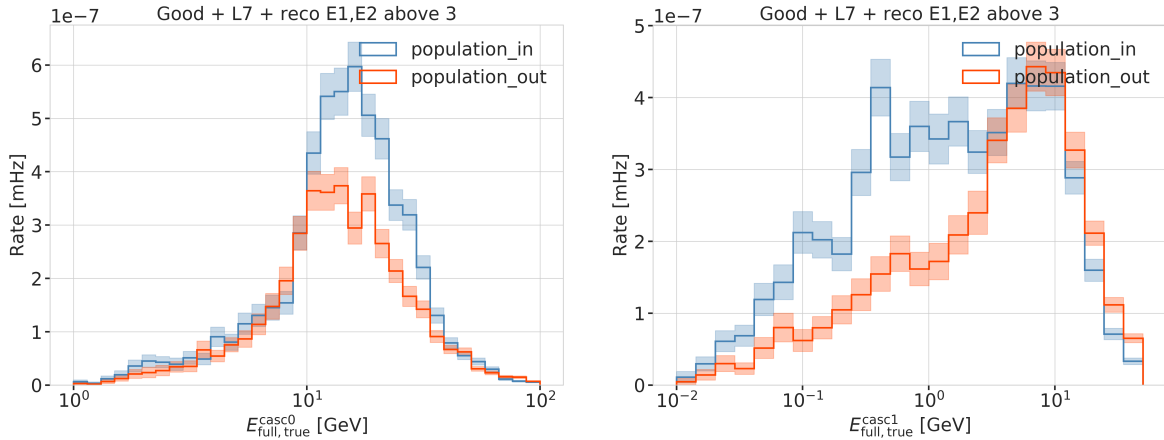


Figure 2.7

below 10 GeV. For the first cascade there is no significant difference between the two populations, but for the second cascade the badly reconstructed population has a larger fraction of events with lower energies and the distribution is almost uniform in the range of 2 GeV to 10 GeV, while the well reconstructed population has a peak around 10 GeV and falls off faster towards lower energies. This is a strong indication that the main reason for the bad reconstruction is the low energy of the second cascade.

Despite the fact that the split into the two populations was very rudimentary, it is clear that the main reason for the bad reconstruction is the low energy of the second cascade, while other factors, like the position of the second cascade, or the potentially bad input seed direction are also contributing to the bad reconstruction. For a more thorough investigation, a more sophisticated separation would be needed, but this is sufficient to conclude that the main reason for the bad reconstruction is the low energy of the second cascade.

circle back to the energy distributions I showed somewhere else, and state how the cascade energies are distributed in general (ORANGE)

## 2.2 Double Cascade Classification

### Missing Points

- ▶ Briefly mention MuMillipede "reconstruction" (depending on how deep I want to go into the classifier I tested?)
- ▶ Calculated variables to input the classifier (distributions?) I guess some examples might do?
- ▶ Cuts applied to make sure the classifier is trained on well reconstructed events (energy, length, true, reco..)
- ▶ Tested classifier (BDT) versions and their performance
- ▶ takeaway? (not sure how to deal with the caveat of the weight being kind of wrong for these..)

## 2.3 Generic Double Cascade Performance

### Ideas:

- ▶ why do these checks again with the model independent samples? (controllable parameter space and distributions, especially energy and length)
- ▶ benchmark some edge cases (e.g. "best case" of up-going string centered, purely horizontal, and realistic case)
- ▶ investigate where the reconstructions breaks down (in terms of cascade energies, which are the main factor as shown before)

### 2.3.1 Idealistic Performance

- ▶ for the perfect edge case of the event being directly on top of a DeepCore string with an up-going direction the length can be very well reconstructed above a true length of around 20 m
- ▶ 2-d histogram shows that up to a true decay length of  $\sim 210$  m, there is no under-estimation of the length
- ▶ this means that the under-estimation observed before is only possible if there is no DOMs in between the two cascades
- ▶ this makes a lot of sense, since DOMs being present, but not observing any light is affecting the light expectation that goes into the reconstruction likelihood and therefore makes these hypotheses less likely and therefore incompatible with the data
- ▶ do I want more detailed plots here? I feel like this is enough..

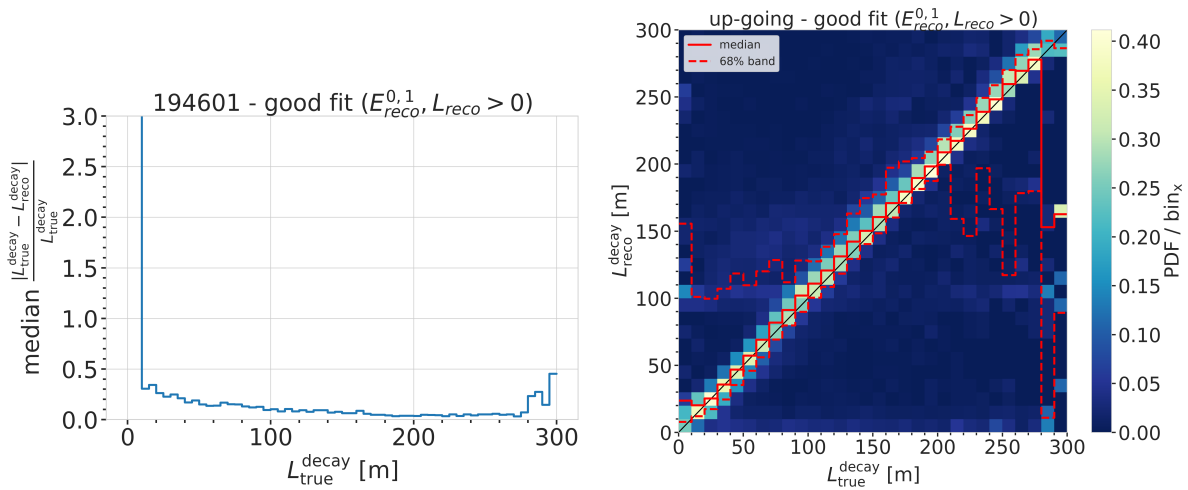


Figure 2.8

fix caption of this figure  
(RED)

### 2.3.2 Realistic Performance

#### Energy/Decay Length Resolution

#### 2-D Histograms

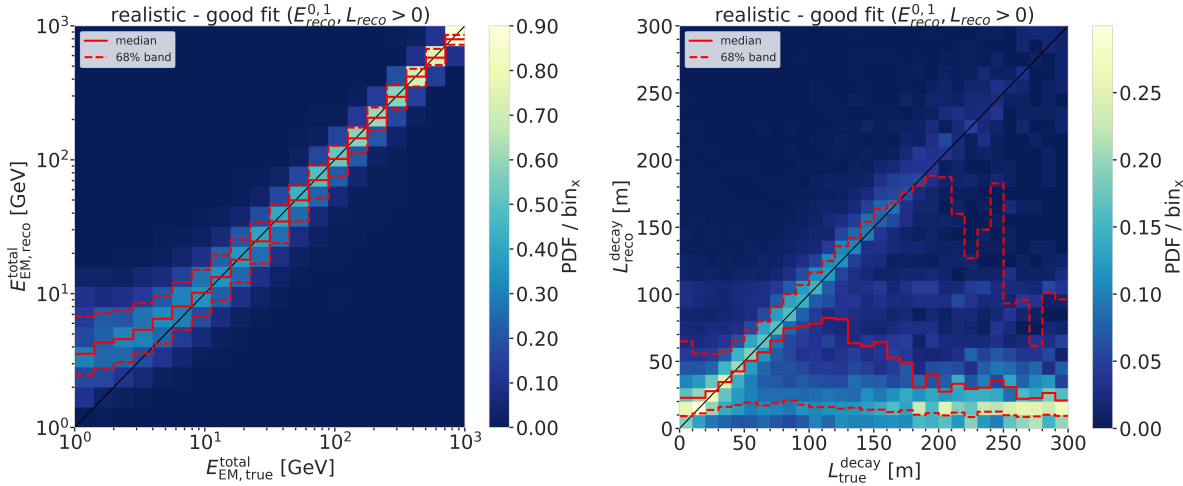
#### Things to mention about the 2d-hists:

- ▶ total energy resolution looks very good, above 10 GeV it's almost unbiased and the 1-sigma resolution band is below 20 %

describe the "good fit" selection when I first show plots that use it (ORANGE)

add some 1D resolution plots (ORANGE)

- ▶ individual cascade resolutions mirror this behavior, but are starting to stabilize in energy at lower energies around 5 GeV to 6 GeV with a broader resolution band of 50 %, but reducing drastically with increasing energy (down to 20 % at 100 GeV)
- ▶ interestingly, the second cascade energy reconstruction performs slightly worse, although they have the same energy ranges. This could hint at an asymmetry in the reconstruction process (might relate to how the two cascades are parameterized) or be due to the different positions and the dominantly up-going direction used in the sampling combined with the DOMs looking down (relate this to the sampling distributions explained/shown in the previous chapter)
- ▶ the decay length resolution looks much worse. In the region between 20 m and 80 m it's roughly unbiased, but 1-sigma resolution band is quite wide with a lot of outliers towards short reconstructed lengths. Below 20 m the reconstructed lengths are always over-estimating the true and above 80 m a population of events start to dominate where the decay lengths isn't getting reconstructed at all, which might indicate that one of the cascades wasn't observed. (Relate to the fact that this marginalizes over all energies, meaning also all events which have one cascade with very low energy are included here.)
- ▶ another interesting feature is the band of reconstructed lengths around 100 m, which is probably related to the spacing between most of the strings, which favors the reconstruction to be around this value, because that's the distance at which light can be observed, just from the fact that the DOMs are spaced at this distance (for low energetic cascades, this can dominate the reconstruction)

**Figure 2.9**

fix caption of this figure  
(RED)

fix caption of this figure  
(RED)

#### Energy Resolution Things to mention about the energy resolution:

- ▶ Here it can be seen more clearly how the median total energy resolution starts to stabilize around 0.0 at 10 GeV, while for lower energies the reconstruction is over-estimating the true energy. This is a known behavior of energy reconstructions in IceCube, which is mainly due to a selection effect. Only events with a certain amount of light can be reconstructed, which means that the ones with true small energies that are still in the sample are events with over average light production

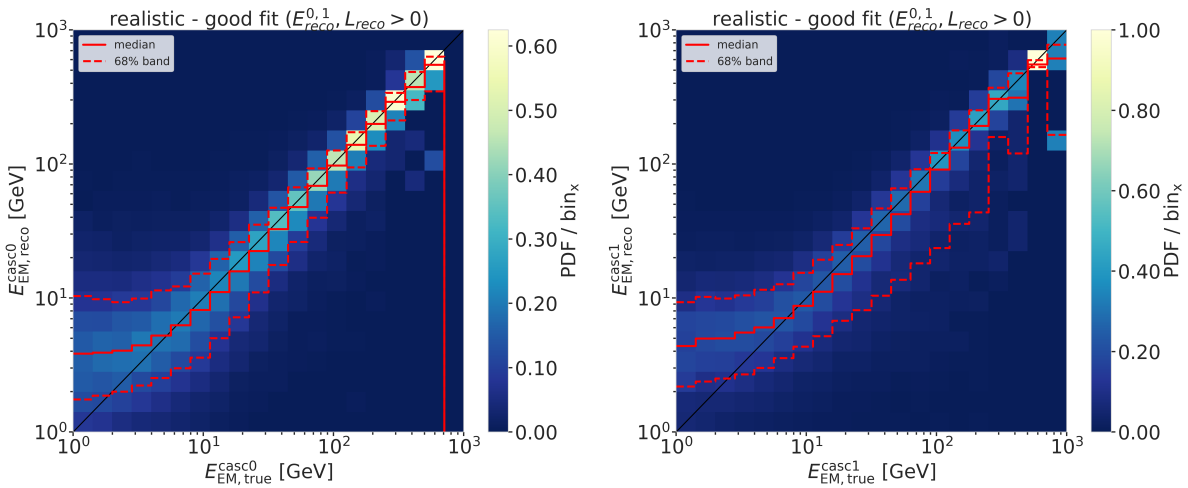


Figure 2.10

due to fluctuations or other effects?

**Decay Length Resolution** Things to mention about the decay length resolution:

- As already mentioned before, the decay length resolution is much worse than the energy resolutions. Figure 2.12 also shows that the median is below 0.0 for short true length and above 0.0 and approaching 1.0 for long true lengths.
- To investigate whether this is really due to the fact that one of the cascades is not observed, the decay length resolution was plotted against the total energy of the event and the minimum energy of the two cascades Figure 2.13.
- It can be seen that the median of the decay length resolution stabilizes at 0.0 for a total energy above 20 GeV, but the spread of the distribution is still quite large with a 1-sigma band of 80 % to 100 %.
- From the plot against the minimum energy it can be seen that the decay length resolution starts to be unbiased for a minimum energy of the cascades of 7 GeV, with an equivalently large spread.
- A preliminary takeaway from this is that the decay length reconstruction is not reliable at all for events with a total energy below 20 GeV or a minimum cascade energy below 7 GeV.

fix caption of this figure  
(RED)

fix caption of this figure  
(RED)

fix caption of this figure  
(RED)

### 2.3.3 Low Energy Event Selection Efficiency

Discussion ideas:

- Show energy, length distribution across the different levels?
- Show efficiency as table across the different levels (MC events + fraction?)
- Compare this to BG efficiency? (maybe rather for the discussion)
- At which level does the selection reduce the HNL the most?
- Is there a place to improve the HNL selection? (Might have to factor in the BG efficiency, as well..)

Make plot to show efficiency of the OscNext selection for HNL events.  
(ORANGE)

Plot energy (true total) and true decay length across the different levels  
(ORANGE)

Make table with the rates across the different levels for benchmark mass/mixing  
(ORANGE)

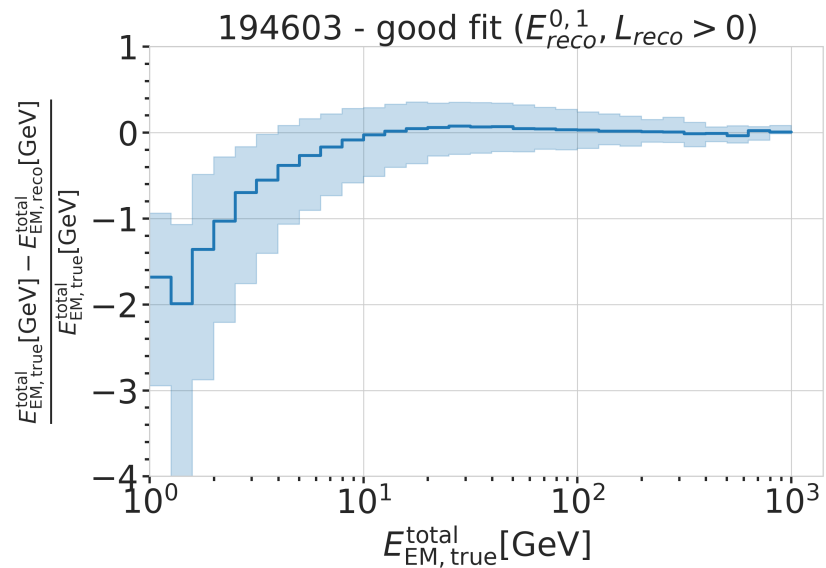


Figure 2.11

- What of this might change with Upgrade? (maybe rather for the discussion)

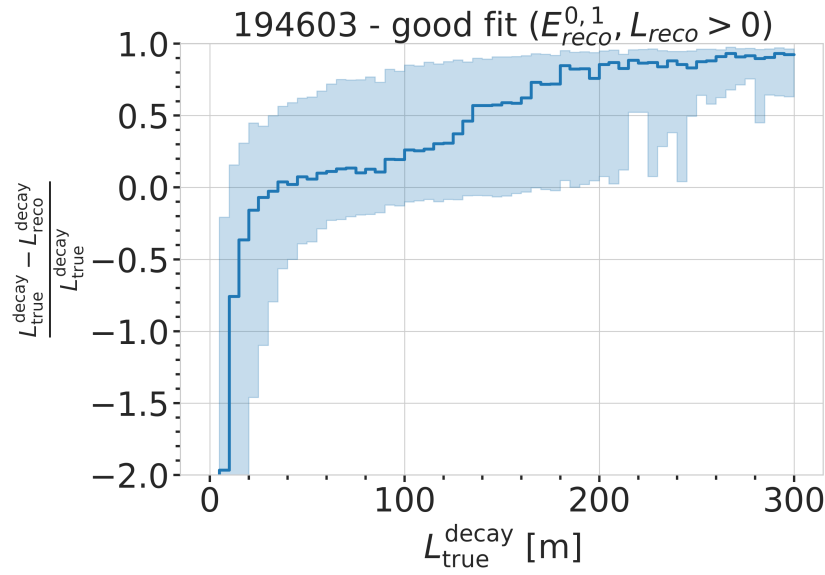


Figure 2.12

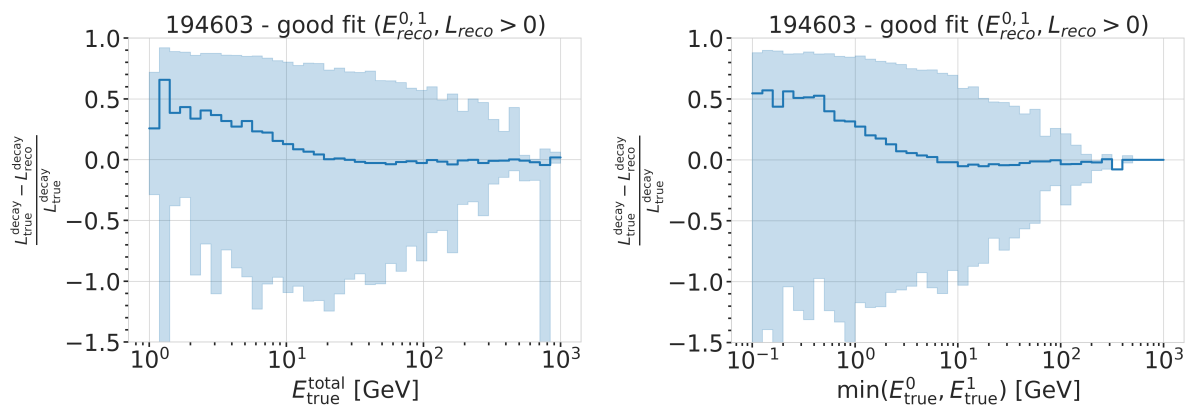


Figure 2.13



# Bibliography

Here are the references in citation order.

- [1] C. N. Yang and R. L. Mills. "Conservation of Isotopic Spin and Isotopic Gauge Invariance". In: *Physical Review* 96.1 (Oct. 1954), pp. 191–195. doi: [10.1103/PhysRev.96.191](https://doi.org/10.1103/PhysRev.96.191) (cited on page 1).
- [2] S. Weinberg. "A Model of Leptons". In: *Phys. Rev. Lett.* 19 (21 Nov. 1967), pp. 1264–1266. doi: [10.1103/PhysRevLett.19.1264](https://doi.org/10.1103/PhysRevLett.19.1264) (cited on page 1).
- [3] S. L. Glashow. "Partial-symmetries of weak interactions". In: *Nuclear Physics* 22.4 (Feb. 1961), pp. 579–588. doi: [10.1016/0029-5582\(61\)90469-2](https://doi.org/10.1016/0029-5582(61)90469-2) (cited on page 1).
- [4] R. Jackiw. "Physical Formulations: Elementary Particle Theory. Relativistic Groups and Analyticity. Proceedings of the eighth Nobel Symposium, Aspenäsgården, Lerum, Sweden, May 1968. Nils Svartholm, Ed. Interscience (Wiley), New York, and Almqvist and Wiksell, Stockholm, 1969. 400 pp., illus. \$31.75." In: *Science* 168.3936 (1970), pp. 1196–1197. doi: [10.1126/science.168.3936.1196.b](https://doi.org/10.1126/science.168.3936.1196.b) (cited on page 1).
- [5] P. Higgs. "Broken symmetries, massless particles and gauge fields". In: *Physics Letters* 12.2 (1964), pp. 132–133. doi: [https://doi.org/10.1016/0031-9163\(64\)91136-9](https://doi.org/10.1016/0031-9163(64)91136-9) (cited on page 1).
- [6] M. Gell-Mann. "A Schematic Model of Baryons and Mesons". In: *Resonance* 24 (1964), pp. 923–925 (cited on page 1).
- [7] G. Zweig. "An SU(3) model for strong interaction symmetry and its breaking. Version 2". In: *DEVELOPMENTS IN THE QUARK THEORY OF HADRONS. VOL. 1. 1964 - 1978*. Ed. by D. B. Lichtenberg and S. P. Rosen. Feb. 1964, pp. 22–101 (cited on page 1).
- [8] D. J. Gross and F. Wilczek. "Ultraviolet Behavior of Non-Abelian Gauge Theories". In: *PRL* 30.26 (June 1973), pp. 1343–1346. doi: [10.1103/PhysRevLett.30.1343](https://doi.org/10.1103/PhysRevLett.30.1343) (cited on page 1).
- [9] C. Giunti and C. W. Kim. *Fundamentals of Neutrino Physics and Astrophysics*. Oxford University Press, Mar. 2007 (cited on page 1).
- [10] M. D. Schwartz. *Quantum Field Theory and the Standard Model*. Cambridge University Press, 2013 (cited on page 1).
- [11] A. Terliuk. "Measurement of atmospheric neutrino oscillations and search for sterile neutrino mixing with IceCube DeepCore". PhD thesis. Berlin, Germany: Humboldt-Universität zu Berlin, Mathematisch-Naturwissenschaftliche Fakultät, 2018. doi: [10.18452/19304](https://doi.org/10.18452/19304) (cited on pages 3, 10).
- [12] M. Thomson. *Modern particle physics*. Cambridge [u.a.]: Cambridge University Press, 2013, XVI, 554 S. (Cited on page 3).
- [13] R. Davis, D. S. Harmer, and K. C. Hoffman. "Search for Neutrinos from the Sun". In: *Phys. Rev. Lett.* 20 (21 May 1968), pp. 1205–1209. doi: [10.1103/PhysRevLett.20.1205](https://doi.org/10.1103/PhysRevLett.20.1205) (cited on page 4).
- [14] Y. Fukuda et al. "Evidence for Oscillation of Atmospheric Neutrinos". In: *Phys. Rev. Lett.* 81 (8 Aug. 1998), pp. 1562–1567. doi: [10.1103/PhysRevLett.81.1562](https://doi.org/10.1103/PhysRevLett.81.1562) (cited on page 4).
- [15] Q. R. Ahmad and other. "Direct Evidence for Neutrino Flavor Transformation from Neutral-Current Interactions in the Sudbury Neutrino Observatory". In: *Phys. Rev. Lett.* 89 (1 June 2002), p. 011301. doi: [10.1103/PhysRevLett.89.011301](https://doi.org/10.1103/PhysRevLett.89.011301) (cited on page 4).
- [16] M. Tanabashi et al. "Review of Particle Physics". In: *Phys. Rev. D* 98 (3 Aug. 2018), p. 030001. doi: [10.1103/PhysRevD.98.030001](https://doi.org/10.1103/PhysRevD.98.030001) (cited on pages 4, 8, 11).
- [17] M. Aker et al. "Direct neutrino-mass measurement with sub-electronvolt sensitivity". In: *Nature Phys.* 18.2 (2022), pp. 160–166. doi: [10.1038/s41567-021-01463-1](https://doi.org/10.1038/s41567-021-01463-1) (cited on page 4).

- [18] S. Alam et al. "Completed SDSS-IV extended Baryon Oscillation Spectroscopic Survey: Cosmological implications from two decades of spectroscopic surveys at the Apache Point Observatory". In: *Phys. Rev. D* 103 (8 Apr. 2021), p. 083533. doi: [10.1103/PhysRevD.103.083533](https://doi.org/10.1103/PhysRevD.103.083533) (cited on page 4).
- [19] N. Aghanim et al. "Planck2018 results: VI. Cosmological parameters". In: *Astronomy & Astrophysics* 641 (Sept. 2020), A6. doi: [10.1051/0004-6361/201833910](https://doi.org/10.1051/0004-6361/201833910) (cited on page 4).
- [20] P. Coloma et al. "GeV-scale neutrinos: interactions with mesons and DUNE sensitivity". In: *Eur. Phys. J. C* 81.1 (2021), p. 78. doi: [10.1140/epjc/s10052-021-08861-y](https://doi.org/10.1140/epjc/s10052-021-08861-y) (cited on pages 8, 13, 15).
- [21] M. Honda et al. "Atmospheric neutrino flux calculation using the NRLMSISE-00 atmospheric model". In: *Phys. Rev. D* 92 (2 July 2015), p. 023004. doi: [10.1103/PhysRevD.92.023004](https://doi.org/10.1103/PhysRevD.92.023004) (cited on page 9).
- [22] A. Fedynitch et al. "Calculation of conventional and prompt lepton fluxes at very high energy". In: *European Physical Journal Web of Conferences*. Vol. 99. European Physical Journal Web of Conferences. Aug. 2015, p. 08001. doi: [10.1051/epjconf/20159908001](https://doi.org/10.1051/epjconf/20159908001) (cited on page 9).
- [23] J. A. Formaggio and G. P. Zeller. "From eV to EeV: Neutrino cross sections across energy scales". In: *Rev. Mod. Phys.* 84 (3 Sept. 2012), pp. 1307–1341. doi: [10.1103/RevModPhys.84.1307](https://doi.org/10.1103/RevModPhys.84.1307) (cited on page 10).
- [24] S. Bilenky and B. Pontecorvo. "Lepton mixing and neutrino oscillations". In: *Physics Reports* 41.4 (1978), pp. 225–261. doi: [10.1016/0370-1573\(78\)90095-9](https://doi.org/10.1016/0370-1573(78)90095-9) (cited on page 11).
- [25] P. A. M. Dirac. "The Quantum Theory of the Emission and Absorption of Radiation". In: *Proceedings of the Royal Society of London Series A* 114.767 (Mar. 1927), pp. 243–265. doi: [10.1098/rspa.1927.0039](https://doi.org/10.1098/rspa.1927.0039) (cited on page 11).
- [26] T. Yanagida. "Horizontal Symmetry and Masses of Neutrinos". In: *Progress of Theoretical Physics* 64.3 (Sept. 1980), pp. 1103–1105. doi: [PTP.64.1103](https://doi.org/10.1143/PTP.64.1103) (cited on page 12).
- [27] P. Astier et al. "Search for heavy neutrinos mixing with tau neutrinos". In: *Phys. Lett. B* 506 (2001), pp. 27–38. doi: [10.1016/S0370-2693\(01\)00362-8](https://doi.org/10.1016/S0370-2693(01)00362-8) (cited on page 12).
- [28] R. Acciari et al. "New Constraints on Tau-Coupled Heavy Neutral Leptons with Masses mN=280–970 MeV". In: *Phys. Rev. Lett.* 127.12 (2021), p. 121801. doi: [10.1103/PhysRevLett.127.121801](https://doi.org/10.1103/PhysRevLett.127.121801) (cited on page 12).
- [29] J. Orloff, A. N. Rozanov, and C. Santoni. "Limits on the mixing of tau neutrino to heavy neutrinos". In: *Phys. Lett. B* 550 (2002), pp. 8–15. doi: [10.1016/S0370-2693\(02\)02769-7](https://doi.org/10.1016/S0370-2693(02)02769-7) (cited on page 12).
- [30] I. Boiarska et al. "Blast from the past: constraints from the CHARM experiment on Heavy Neutral Leptons with tau mixing". In: (July 2021) (cited on page 12).
- [31] P. Abreu et al. "Search for neutral heavy leptons produced in Z decays". In: *Z. Phys. C* 74 (1997). [Erratum: *Z.Phys.C* 75, 580 (1997)], pp. 57–71. doi: [10.1007/s002880050370](https://doi.org/10.1007/s002880050370) (cited on page 12).
- [32] P. Coloma et al. "Double-Cascade Events from New Physics in Icecube". In: *Phys. Rev. Lett.* 119.20 (2017), p. 201804. doi: [10.1103/PhysRevLett.119.201804](https://doi.org/10.1103/PhysRevLett.119.201804) (cited on page 13).
- [33] P. Coloma. "Icecube/DeepCore tests for novel explanations of the MiniBooNE anomaly". In: *Eur. Phys. J. C* 79.9 (2019), p. 748. doi: [10.1140/epjc/s10052-019-7256-8](https://doi.org/10.1140/epjc/s10052-019-7256-8) (cited on page 13).
- [34] R. Abbasi et al. "Measurement of Astrophysical Tau Neutrinos in IceCube's High-Energy Starting Events". In: *arXiv e-prints* (Nov. 2020) (cited on page 17).
- [35] M. Usner. "Search for Astrophysical Tau-Neutrinos in Six Years of High-Energy Starting Events in the IceCube Detector". PhD thesis. Berlin, Germany: Humboldt-Universität zu Berlin, Mathematisch-Naturwissenschaftliche Fakultät, 2018. doi: [10.18452/19458](https://doi.org/10.18452/19458) (cited on page 17).
- [36] P. Hallen. "On the Measurement of High-Energy Tau Neutrinos with IceCube". MA thesis. Aachen, Germany: RWTH Aachen University, 2013 (cited on page 17).
- [37] N. Whitehorn, J. van Santen, and S. Lafebre. "Penalized splines for smooth representation of high-dimensional Monte Carlo datasets". In: *Computer Physics Communications* 184.9 (2013), pp. 2214–2220. doi: <https://doi.org/10.1016/j.cpc.2013.04.008> (cited on page 17).
- [38] M. G. Aartsen et al. "Energy Reconstruction Methods in the IceCube Neutrino Telescope". In: *JINST* 9 (2014), P03009. doi: [10.1088/1748-0221/9/03/P03009](https://doi.org/10.1088/1748-0221/9/03/P03009) (cited on page 17).

- [39] R. Abbasi et al. “Low energy event reconstruction in IceCube DeepCore”. In: *Eur. Phys. J. C* 82.9 (2022), p. 807. doi: [10.1140/epjc/s10052-022-10721-2](https://doi.org/10.1140/epjc/s10052-022-10721-2) (cited on page 18).